



Numerical Prediction of Trailing Edge Noise at Low Reynolds Number with Modified Trailing Edges of a NACA 0015 Airfoil

Mohamed Ibren¹, Amelda Dianne Andan^{1,*}, Waqar Asrar¹

¹ Department of Mechanical Engineering, Kulliyah of Engineering, International Islamic University Malaysia, Kuala Lumpur, 53100, Malaysia

ARTICLE INFO

Article history:

Received 16 October 2023

Received in revised form 17 November 2023

Accepted 14 December 2023

Available online 31 March 2024

Keywords:

Low-Reynolds Number; NACA0015 Airfoil; Aeroacoustics; Trailing-Edge Noise; Serration; Comb

ABSTRACT

Global concern about high noise levels in areas near airports and wind farms has generated interest from various groups due to factors such as potential health problems and dissatisfaction among the local community. To accommodate this worthwhile plan of further reducing overall noise levels, some researchers are working on lowering the contribution of trailing-edge noise. The original scientific contribution of this study lies on understanding the efficiency of various trailing edge designs such as baseline, serrations, comb and comb-serrated, across different angles of attack and Reynolds numbers, while also addressing the limitations of existing geometrical models for trailing edges. The study intends to examine the performance of these different configurations, with an emphasis on their effect on acoustic responses. By utilizing large-eddy simulation and applying the Ffowcs-Williams and Hawkings models for noise prediction, an investigation was conducted to assess the impact of these trailing edge configurations on radiated noise at a low Reynolds number of 1.6×10^5 . The numerical predictions of lift coefficient and surface pressure fluctuations are compared and validated with a published study and experimental data, showing satisfactory results. Further analysis of these study has demonstrated that prominent peaks at lower frequencies ($<10^3$) are observed, which are identified as the characteristic frequencies. Moreover, results showed irregular broadband noise (300 - 600 Hz) with increased noise and shifting peak frequency as angle of attack rose. The serrated trailing edge design notably reduced noise levels by roughly 21 dB, especially for low frequencies. Comb-serration increased high-frequency noise by about 9 dB for angles of attack at 0, -1, and -2°, and achieved a reduction of approximately 9 dB for angles of attack at 1 and 2°. On the other hand, the directivity pattern showed that the maximum noise level is observed to predominantly radiate at an azimuth angle of around 90 degrees for all the cases, ranging from 90° to 270°, indicating that the majority of the source's acoustic energy is being emitted on the suction and pressure sides of the airfoil.

1. Introduction

The Rapid growth of surrounding airports, increase in the wind turbines usage [1] and high level of aircraft generated noise have evoked awareness about noise hazards [2-4]. As a result, strict

* Corresponding author.

E-mail address: ameldadianne@iium.edu.my (Amelda Dianne Binti Andan)

<https://doi.org/10.37934/cfdl.16.8.6494>

measures are being imposed on aviation industries [5-7]. Consequently, this has sparked interest in understanding the fundamental mechanisms of noise generation [2, 8, 9] as well as inventing ways of mitigating radiated noise [4, 5, 10, 12, 13]. This heightened attention is attributed to the fact that noise reduction has emerged as a crucial challenge that cannot be overlooked [11]. These efforts have been deliberated carefully by acoustically tailored materials and/or altering the design configurations [15]. Many researchers have been bio-inspired by nature's silent fliers. For instance, Owls and eagles are considered near silent flight [16, 17] due to three features that makes their feathers soft and non-rigid: comb-like feathers at the leading-edge serrations, a velvet-like fluff on the wing surface, and fringe-like feathers at the trailing edge [18]. On the other hand, this will increase short take-off and landing within small city airports that are close to densely populated area [19].

Solid bodies produce unsteady disturbances (T-S Wave) that initiate transition to turbulence as a result of their motion through a fluid flow. Thereafter, laminar boundary layer may separate depending on the fluid flow conditions. The flow can either attach to the surface or interact after the trailing edge and form a complex wake region [20]. The area enclosed by the separated and reattachment points is known as recirculation zone. This flow parameters significantly dictate the flow physics of low-to-moderate Reynolds numbers [21].

Consequently, as the amplified T-S wave passes the airfoil trailing edge, boundary-layer pressure fluctuations linked to turbulent are aeroacoustically scattered due to the presence of discontinuity such as trailing edge [22]. Therefore, turbulent kinetic energy is converted to a strong acoustic wave that is propagated to the far field in a dipolar or quadrupolar manner, and thus, the noise generated is often referred to as trailing-edge noise [15, 23-27]. This occurs at the large-physical length scale involved relative to the acoustic wavelength, for small-body limit, noise generation is limited by the large-scale vortices [25]. The process is also affected by the presence of adverse pressure gradient, separation region and vortex shedding mechanism near the trailing edge [25]. Separation without reattachment reduces exponentially the noise generated since eddies move into the wake area and do not interact with the trailing edge [2]. In addition to the separation, attached turbulent flow decreases the noise radiated when compared with laminar flow [28]. Therefore, trailing-edge noise is considered very important in the design of wind turbines, submarines, aircrafts and automobiles. [4, 5, 15, 24, 29-33].

Aeroacoustics noise is categorized into airfoil self-noise and turbulent inflow noise [34]. Airfoil self-noise is often known as turbulent-structure interaction noise. Turbulent-structure interaction noise is considered one of the component that contribute as much noise level as the engines especially for the conventional aircraft [35]. For instance, trailing-edge noise, which occurs due to turbulent-boundary layer interaction with the trailing-edge forms one of the main source of airfoil self-noise [2, 5, 32, 36]. The swishing noise generated by wind turbine blades is one of the application where trailing-edge noise is considered dominant, and it can be heard at a reasonable distance from the source [37]. Subsequently, this has influenced the certification process due to a high rate of refusal [4].

Trailing-edge noise prediction techniques proposed and developed are based on analytical and semi-analytical methods [38-46]. Analytical models were based upon physical geometry only whereas semi-analytical depended on extra features such as boundary layer parameters and unsteady surface pressure fluctuations [47]. However, predicting radiated noise around serrated trailing-edge is still unclear due to the complexity of the flow field [48-50]. The initial model proposed to analyze noise generated in the presence of a semi-infinite flat plate with serrated trailing-edge was based on the assumptions of effective frozen boundary layer turbulence [39]. The method predicted that the noise radiated in the presence of serrated trailing-edge at high frequency is less

by approximately $10 \log_{10}[1 + (4h/\lambda)^2]$ dB compared to the unserrated (straight) trailing-edge. The trailing-edge noise prediction is dependent on serration amplitude ($2h$) and spanwise wavelength of the serration (λ). Nevertheless, several researchers [33, 49, 51-56] pointed-out that the model does not give accurate solutions when compared with the measurements, it over-projects maximum noise reduction and does not show increase of the noise beyond cross-over frequency [55]. On the other hand, for more noise reduction to be achieved, another comprehensive study proposed that serration height has to be greater than boundary layer thickness at the trailing-edge ($2h \geq \delta$) where δ is the boundary layer thickness [57]. In spite of the differences shown above, a study [57] still acknowledged Howe's model in that narrower sawtooth is more essential for maximum noise reduction. Moreover, previous study [41] has proposed a new model that is more realistic and consistent with experimental work.

Whereas milestone achievements have been made in understanding flow physics, scattering of acoustic wave and propagations of the noise [38-39, 41-46] there have been incredible interest in developing attenuation tools that can reduce noise generated at the trailing edge [58]. With the aim of mitigating trailing-edge noise, various means of reducing noise are based upon controlling either the surface pressure fluctuations or scattering of the acoustic wave. Accordingly, this has led to the proposal of various trailing-edge noise mitigation methods, which are classified into two groups based on their plan of action: passive and active control methods [59]. Active control methods act on altering the flow structure such as unsteady pressure fluctuations upstream of the trailing-edge, and passive methods attempt to improve the scattering condition by changing the physical and geometrical properties of the trailing-edge [5, 59]. Recently, various passive control techniques such as the use of porous [59-62], brushes [63, 64], serration [41, 48, 56], surface treatment [27, 65], shape optimization [52], morphing [66] and flexible materials [67] were developed and investigated for the purpose of improving aerodynamic performance as well as reducing noise generated at the trailing-edge [62]. In this study, the noise mitigation approach is based on trailing-edge serration, combed trailing-edge and comb-serrated trailing-edge. As a result, the flow structure around the trailing-edge is improved and thus reduces noise generated.

Following the nature of the Owls, the use of serration geometries as a passive tool has been widely investigated by several researchers [41, 48, 56]. Indeed, earlier attempts by several experimental studies have shown that trailing-edge serration is one of the promising passive control technique to decrease trailing-edge noise. One of the studies that was performed at high Reynolds number (1.6 Million) showed that noise can be reduced by about 6 dB. Moreover, when applied to the full-scale wind turbine blades, the noise was successfully decreased by approximately 3 dB at frequency below 1 kHz and increases above 1kHz without significantly affecting the aerodynamic performance [4]. Yet on another work, Investigation at relatively low Reynolds number (200,000 – 830,000) found out that noise can be reduced by about 7 dB at frequency below 2 kHz and an increase in the noise level above this frequency. In addition, the Strouhal number based on boundary-layer thickness that delimits noise increase and decrease was determined to be roughly 1 [57].

Some of the reasons that contribute to the reduction of noise are the capability of this passive method to effectively eliminate vortex-shedding tones [33] as well as suppressing boundary-layer instabilities [68]. The increment of noise at high frequency is associated with turbulence intensity near the sawtooth side edges [53], this noise is amplified with misalignment between the sawtooth edges and the undisturbed wake field [40]. On the other hand, crossflow is proposed to be the main reason of increase in noise at high frequency due to high momentum fluid hitting the sawtooth edges frequently [50]. Another extensive experimental study suggested that increase of noise at high frequency is based on increment of the wall-normal velocity fluctuation at the lower side of the serration [69].

Some of the investigations have shown that cutting serration connected to the main body compared to the flat plate inserts have higher broadband noises due to the presence of bluntness, however, they have also observed that increment of noise at high frequency can be reduced with cutting serration linked to the main body [70]. Furthermore, those broadband noises can be reduced by introducing mesh screens that cover the serration surfaces [70]. Consequently, other variations of the serration have been examined recently, and were shown to be more effective. For instance, with combed-serration, an additional 2 dB noise reduction was observed [37].

Extensive early investigations on porous devices have shown that noise can be reduced significantly [71, 72]. A comprehensive study based on the effects of porous edges applied to a flat plate has shown that trailing-edge noise can be reduced by about 7 dB. This reduction was linked to the absorption and stabilization of the unsteady pressure fluctuations. Moreover, this noise is expected to reduce further whenever the amount of the pores is gradually increased downstream as a result of progressive adjustment of the surface discontinuity [45]. Based on a 2D airfoil experiment that is covered with porous material at the trailing-edge, maximum trailing-edge noise of up to 3 dB can be achieved [73]. In addition, another experimental work demonstrated that porous materials could reduce noise up to 10 dB at low frequency with less effects to the aerodynamic performance [74].

One of the parameters that is commonly used to evaluate the performance of the porous material is resistivity, and it is linked to the pressure drop the porous medium. For instance, low-flow resistivity has been demonstrated to reduce noise at the trailing-edge [4]. Similarly, another study based on cambered airfoil confirmed that noise reduction can be achieved as a result of porous flow resistivity, but they have observed an increase in noise at high frequency due to surface roughness created by the porous medium [75].

Another concept that facilitates fluid-flow structure is porosity, it is related to various parameters such hole size and distribution of the holes. Interestingly, radiated noise can be minimized if airfoil surface is even partially covered with porous medium [19, 60, 76]. It has also been demonstrated that moderate permeability provides the highest noise reduction [61, 77]. Higher permeability has negligible resistance, thus regarded as a shortened chord. Whereas lower permeability behaves like a solid surface, thus giving almost the same results as the solid model. However, for relatively larger hole size, an increase in noise at higher frequency has been reported [75]. The noise generated can be minimized if a smaller pore size with sub-millimeter diameter is utilized. This is because smaller-sized pores can suppress vortex shedding noise and turbulent noise near the trailing edges [77]. With those parameters, the flow oozes through the porous channel and surface. Hence, interfering with the boundary layer and lowers the radiated noise near the trailing edge [77]. Additionally, material selection is an important criterion to achieve significant noise reduction [78]. Moreover, correct placement of the porous region on the airfoil's surface can suppress the vortex roll-up, which will reduce pressure fluctuation and peak swirl velocity; consequently, reducing the generated noise [79]. Furthermore, smooth porosity distribution eliminates sudden changes in the acoustic impedance, which is known to be the dominant cause of the trailing edge noise [34].

On the contrary, some of the parameters that have been reported to increase the noise are pores' surface roughness [19, 79] and layout [19], improper installation [19], low porosity and vibration of the trailing-edge [78]. In addition, porous materials generate noise when air flows over the transition of solid and porous parts. This source increases with the increased permeability [80]. On top of all that, many porous models such as metal foams produced less noise compared to the baseline [78].

Despite direct numerical simulation (DNS) having lesser physical inputs and more accurate results, it is computationally expensive due to the wide range of the length scale needed to be evaluated [80]. Based on the need of high accurate unsteady flow-field solution, the fluid analysis is

performed using scale-resolving computation known as large-eddy simulation (LES). Large-eddy simulation resolves the energy containing eddies (large-scale eddies) directly and makes use of sub-grid scale (SGS) to analyze the effect small-scale eddies [81]. These large-scale eddies are considered to be the most contributor of the acoustic source [25]. In this manuscript, Ffowcs-Williams and Hawkings (FW-H) acoustic analogy is used to determine the far-field pressure fluctuations. This analogy separates computational process into two, which is analyzing the incompressible large-eddy simulation and then the unsteady fluid-flow data are input into the acoustic source term that computes the noise generated at any location from the surface [24, 29]. From the above explanation, this approach needs very accurate results from the unsteady computational fluid dynamic (CFD). Therefore, any fault from the computation of the incompressible large-eddy simulation would completely lead to inaccuracy of the acoustic source term as well as the far-field acoustic solutions [29]. Furthermore, in order to minimize the influence of unsteady flow field within the initial stage, acoustic solutions were performed from a complete converged steady state simulation and a stable unsteady incompressible LES solution.

The computation reported here describes the progress and the use of bio-inspired passive tools to mitigate trailing-edge noise. The investigations were performed around a NACA 0015 airfoil at a chord-based Reynolds number of about 1.6×10^5 , and for varies angles of attack ($-2^\circ < \alpha < 2^\circ$). Both the mean flow variables and the instantaneous quantities are computed and compared with other studies. Additionally, the far-field acoustic results generated from the source term are analyzed and presented accordingly.

2. Numerical Scheme

2.1 Large Eddy Simulation (LES)

For Large eddy simulation (LES) is a method of numerically simulating fluid dynamics and turbulence. It is a type of computational fluid dynamics (CFD) method that filters the governing equations of fluid motion (such as the Navier-Stokes equations) to only solve for the larger, or "eddy," motions while modeling the smaller, "sub-grid scale" motions using a turbulence model [82]. This allows for more accurate simulations of turbulent flows while reducing the computational cost compared to resolving all scales of motion. LES can be applied to various applications, such as meteorology, atmospheric science, aerospace engineering, and many others. The filtered version of this model can be carried out using an explicit method, an implicit method, or a combination of both [81].

The equations that govern the filtered Navier–Stokes and continuity for incompressible flow can be written as; [83]:

$$\frac{\partial}{\partial t}(\rho \underline{u}_i) + \frac{\partial}{\partial x_j}(\rho \underline{u}_i \underline{u}_j) = \frac{\partial}{\partial x_j}(\sigma_{ij}) - \frac{\partial p}{\partial x_i} - \frac{\partial \tau_{ij}}{\partial x_j} \quad (1)$$

$$\frac{\partial \rho}{\partial t} + \frac{\partial}{\partial x_i}(\rho \underline{u}_i) = 0 \quad (2)$$

Where σ_{ij} is the stress tensor, it is interpreted as follows.

$$\sigma_{ij} = \left[\mu \left(\frac{\partial u_i}{\partial x_j} + \frac{\partial u_j}{\partial x_i} \right) \right] - \frac{2}{3} \mu \frac{\partial u_i}{\partial x_i} \delta_{ij} \quad (3)$$

And τ_{ij} is the subgrid-scale (SGS) stress tensor illustrated as:

$$\tau_{ij} = \rho \underline{u_i u_j} - \rho \underline{u_i} \underline{u_j} \quad (4)$$

Nonetheless, the subgrid-scale stress tensor is unknown and thus modeled based on isotropic assumptions as shown by Eq. (5)

$$\tau_{ij} - \frac{1}{3} \tau_{kk} \delta_{ij} = -2\nu_{sgs} \underline{S}_{ij} \quad (5)$$

Where ν_{sgs} is the subgrid-scale kinematic viscosity and \underline{S}_{ij} is the strain rate from the smallest resolved eddies. The rate of strain tensor is defined as

$$\underline{S}_{ij} = \frac{1}{2} \left(\frac{\partial u_i}{\partial x_j} + \frac{\partial u_j}{\partial x_i} \right) \quad (6)$$

In addition, the subgrid-scale kinematic viscosity is undetermined and thus becomes the variable to be evaluated. Based on the original Smagorinsky method [84], SGS viscosity is computed as follows

$$\nu_{sgs} = C_s \underline{\Delta}^2 |\underline{S}| \quad (7)$$

Where C_s is the model is constant, also referred to as Smagorinsky coefficient. It describes the ratio of the cell size that gives the average eddy in a cell; it has a value ranging from 0 to 1 because it is expected to be less than the cell size. The second term on the right side of Eq. (7) ($\underline{\Delta}$) is the subgrid filter width, this defines the mesh size. Lastly, $|\underline{S}|$ is the modulus of strain rate tensor, equivalent to $\sqrt{2\underline{S}_{ij}\underline{S}_{ij}}$.

Following the computation of subgrid-scale kinematic viscosity, subgrid-scale stress tensor can now be presented as shown by Eq. (8)

$$\tau_{ij} - \frac{1}{3} \tau_{kk} \delta_{ij} = -2C_s \underline{\Delta}^2 |\underline{S}| \underline{S}_{ij} \quad (8)$$

However, the optimum C_s value varies for each part of the flow and must be reduced near solid walls in order to minimize the numerical dissipation introduced by the sub-grid scale model, this is particularly the case for wind turbine blades where the surface fluctuations are assumed to be the main acoustic sources. Therefore, the dynamic Smagorinsky method can be used [85].

In this model an extra filter level known as the test filter ($\tilde{\Delta}$) is used in combination with the sub-grid scale filter level, in order to estimate a value of $C_{s,new}$, which is a function of time and space [86]. Following Germano's [85] evaluation, the two filters were compared as follows.

$$\tilde{L}_{ij} = \underline{u_i u_j} - \tilde{u}_i \tilde{u}_j \quad (9)$$

Each where \tilde{L}_{ij} can be computed using resolved eddies in a cell as shown by Eq. (10)

$$\tilde{L}_{ij} = 2C_{s,new} \underline{\Delta} M_{ij} \quad (10)$$

Each where M_{ij} is defined as;

$$M_{ij} = \left(\frac{\tilde{\Delta}}{\underline{\Delta}}\right)^2 \widetilde{[S][S]_{ij}} \quad (11)$$

Moreover, the new model constant ($C_{s,new}$) that provide stable solution during the analysis is presented by Eq. (12)

$$C_{s,new} \underline{\Delta}^2 = \frac{L_{ij} M_{ij}}{M_{ij} M_{ij}} \quad (12)$$

2.2 Large Eddy Simulation (LES)

Lighthill's theory, also known as Lighthill's acoustic analogy or Lighthill's method [87, 88], is a mathematical framework developed for predicting the noise generated by turbulent flows. It represents the sound generated by turbulent flows as the product of a source term and a propagation term. The theory provides a way to calculate the sound pressure level (SPL) and the sound power level (SWL) for different types of turbulent flows, such as jet and boundary layer flows.

The inability of Lighthill's theory to account for moving surfaces and volume [86] has allowed Ffowcs Williams and Hawkings theory to make use of non-stationary control surfaces [81]. This has extended the application of Lighthill's theory to a rotating source.

The Ffowcs Williams and Hawkings equation can be written as [89]:

$$\frac{1}{C_0^2} \frac{\partial^2 p'}{\partial t^2} - \nabla^2 p' = \frac{\partial^2}{\partial x_i \partial x_j} \{T_{ij} H(f)\} - \frac{\partial}{\partial x_i} \{[P_{ij} n_j + \rho u_i (u_n - v_n)] \delta(f)\} + \frac{\partial}{\partial t} \{[\rho_0 v_n + \rho (u_n - v_n)] \delta(f)\} \quad (13)$$

Where f describes the non-stationary surfaces ($f < 0$ inside part, $f = 0$ on the surface and $f > 0$ outside part), $\delta(f)$ is the Dirac delta function and $H(f)$ is the Heaviside function. u_n and v_n are the fluid and surface velocity normal to the surface. p' is the pressure fluctuation at the far-field observer's location.

The three expressions on the right side of Eq. (13) can be defined as additional acoustic sources. The first term describes the quadrupole source with four lobes; it is related to the velocity fluctuation outside of the surface. This source has very little contribution to a low Reynolds number and thus can be neglected. The second term defines a dipole source with two lobes of directivity. These sources

are generated due to the forces acting on the surface of the body and for this reason, it is also referred to as loading noise. The last term is monopole with a single lobe of directivity. These sources are related to the geometry of the model such as the thickness of the wing hence known as thickness noise [86].

Acoustic pressure fluctuations at any receiver location can be evaluated by the combination of loading (p'_L) and thickness noise (p'_T). Considering low flow velocity, the quadrupole sources are neglected from Eq. (13). Loading and thickness noises are computed as shown by Eq. (15) and Eq. (16).

$$p' = p'_L + p'_T \quad (14)$$

$$4\pi p'_L(x, t) = \frac{1}{C_0} \int_{f=0} \left[\frac{\dot{L}_r}{r(1-M_r)^2} \right]_{ret} ds + \int_{f=0} \left[\frac{L_r - L_M}{r^2(1-M_r)^2} \right]_{ret} ds + \frac{1}{C_0} \int_{f=0} \left[\frac{L_r \{r\dot{M}_r + C_0(M_r - M^2)\}}{r^2(1-M_r)^3} \right]_{ret} ds \quad (15)$$

$$4\pi p'_T(x, t) = \int_{f=0} \left[\frac{\rho_0(\dot{U}_n + U_n)}{r(1-M_r)^2} \right]_{ret} ds + \frac{1}{C_0} \int_{f=0} \left[\frac{\rho_0 U_n \{r\dot{M}_r + C_0(M_r - M^2)\}}{r^2(1-M_r)^3} \right]_{ret} ds \quad (16)$$

Where U_i and L_i are defined as.

$$U_i = v_i + \frac{\rho}{\rho_0} (u_i - v_i) \quad (17)$$

$$L_i = P_{ij} \delta_{ij} n_j + \rho u_i (u_n - v_n) \quad (18)$$

The sound pressure variations that are generated by turbulent flows are much weaker than the aerodynamic pressure variations in the far field, and the wavelength of the sound is much longer compared to the size of the turbulent eddies that create the acoustic disturbances. [81]. As a result, to effectively model the noise sources, it requires fine discretization of the domain, which makes Direct Numerical Simulation (DNS) computationally intensive and not often used for simulating complex 3D fluid flows, such as full-scale turbines [86].

3. Computational Methods

3.1 Model

The NACA 0015 airfoil is a symmetric, low-drag option that is commonly used in low-speed applications such as wind turbines and unmanned aerial vehicles (UAVs). Its simple shape makes it easy to manufacture and maintain, making it a popular choice for many applications. In this study, it has a symmetric shape with a chord length of 0.15 meters and a span of 0.296 meters as shown in Figure 1. The design of the model includes a blunt trailing edge in order to facilitate and simplify the process of meshing during manufacturing or analysis. It was determined that a three-dimensional

analysis should be conducted due to the limited number of three-dimensional computational studies that can be found in the existing literature. Similarly, while a three-dimensional analysis yields relatively precise results, it also requires a greater amount of computational time when compared to using a two-dimensional model. Additionally, it is generally believed that three-dimensional flows are less affected by three-dimensional disturbances at high Reynolds numbers [90]. However, in this study, the analysis is being conducted at relatively low Reynolds numbers, so this may not be the case.

In addition to the baseline NACA 0015 airfoil, the study also examines other trailing edge configurations, including serrated, comb and comb-serrated, as displayed in Figure 2. The parameters employed for the serration, comb, and comb-serration configurations in this study are based on established references [45, 53]. These configurations are a result of modifications made to the airfoil's trailing-edge, located around 30% from the trailing edge. For instance, the serrated model involved the addition of sawtooth-like projections to the airfoil surface, with serration height, wavelength, and angle parameters of 38.55mm, 8mm, and 6 degrees, respectively. The comb modification consisted of parallel ridges with a comb height of 38.55mm and a comb spacing of 5mm. Additionally, the comb-serrated configuration was a combination of both serrated and comb configurations and was defined by the parameters of serration height (38.55mm), serration wavelength (6.5mm), comb height (38.55mm), and comb spacing (1mm). The aim of this examination is to assess the impact of these modifications on the radiated noise over the airfoil surfaces, thereby expanding our understanding of how airfoil trailing edge modifications can impact acoustic wave patterns.

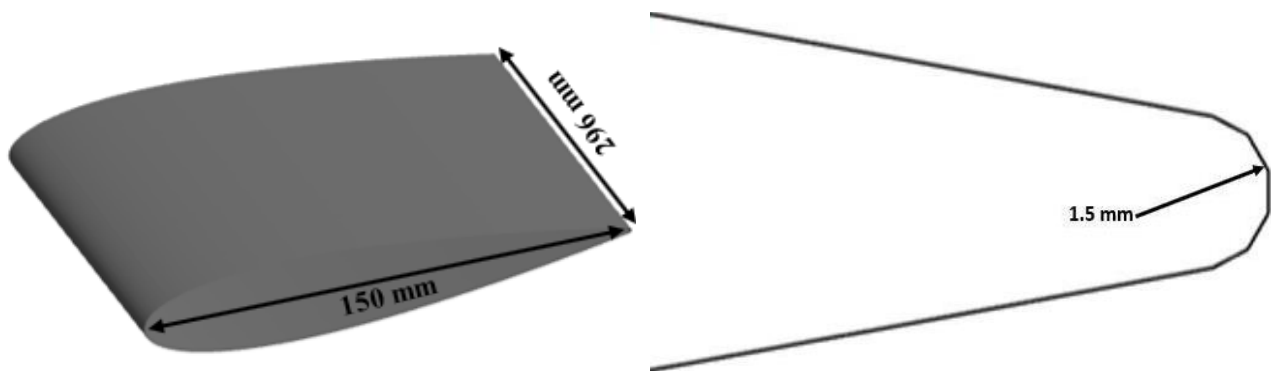
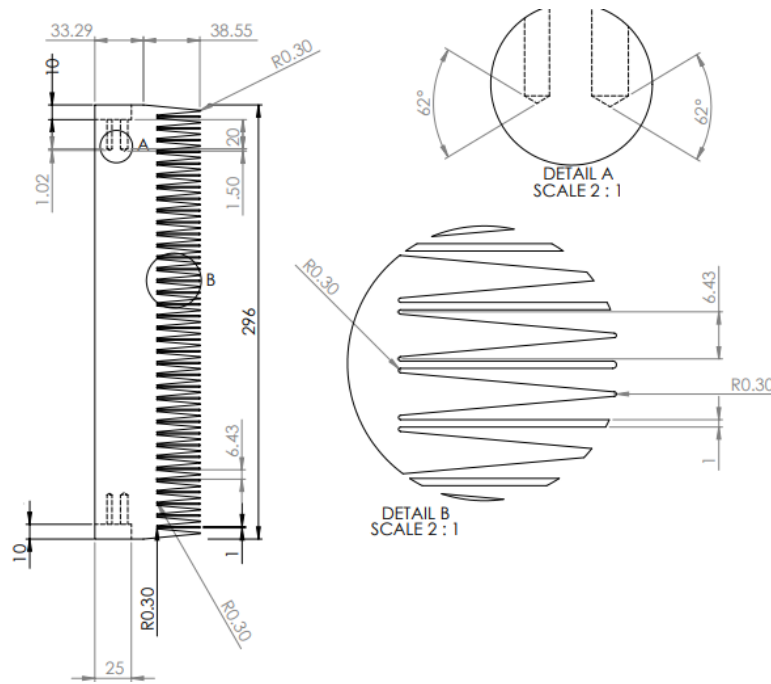


Fig. 1. Geometry of NACA0015 airfoil used in this study



(c)

Fig. 2. Geometry of all the trailing-edge sections used in this study
(a) Serration trailing edge (b) Combed trailing edge (c) Comb-Serrated trailing edge

3.2 Mesh Analysis

The computational domain, defined by the boundaries and initial conditions of the problem, is discretized into a finite number of points called a computational grid. The size and shape of the computational domain can vary depending on the specific problem and the desired level of detail in the simulation. The choice of the computational domain can have a significant impact on the accuracy and efficiency of the simulation. The computational domain represented in Figure 3 was used to study the flow field numerically. It extended 15 airfoil chords upstream, above, and below the airfoil's surface. Additionally, it extended 30 airfoil chords downstream to capture the wake region and ensure a uniform freestream condition at the inlet. The mesh is made up of three parts. The first shell is used for the most detailed mesh near the walls, as it is closest to the boundary layer region. This improves the resolution of the boundary layer. The remaining shells are divided and placed next to each other following the first shell. This division provides an easy way to have a well-distributed and detailed mesh around the area of most interest. The selection of the unstructured C-H grid topology is depicted in Figure 4. The value was found to be approximately 0.9, which is indicative of good wall resolution as it accurately captures boundary layer effects, particularly in the viscous sub-layer region.

The computational mesh used for both analyzing fluid flow near the airfoil surfaces and studying acoustic propagation is the same. To accurately capture the airfoil's surfaces and far-field observer locations, the cell sizes were decreased to around 2 mm. This relatively finer grid improves the accuracy of the computational results. Additionally, using a finer mesh allows for the capture of a broader spectrum of high frequencies.

Considering the main points of focus are the airfoil surfaces, the cell sizes are reduced to about 2mm. A relatively finer grid at those locations enhances the accuracy of the computational outputs. Likewise, finer mesh allows the spectrum of high frequencies to be captured. Similarly, the

computational mesh for a serrated, comb, or comb-serrated model typically employs an unstructured grid approach. The mesh refinement is done in areas close to the trailing edge, due to the complex geometry and boundaries of the physical domain. The mesh refinement allows the grid to accurately capture important geometric and flow features such as sharp edges, narrow gaps, or high gradients. For instance, in a serrated configuration, a sawtooth-like triangular shape is positioned between the serration surfaces to accurately represent the complex geometry of the trailing-edge. This approach ensures a more precise representation and computational results.

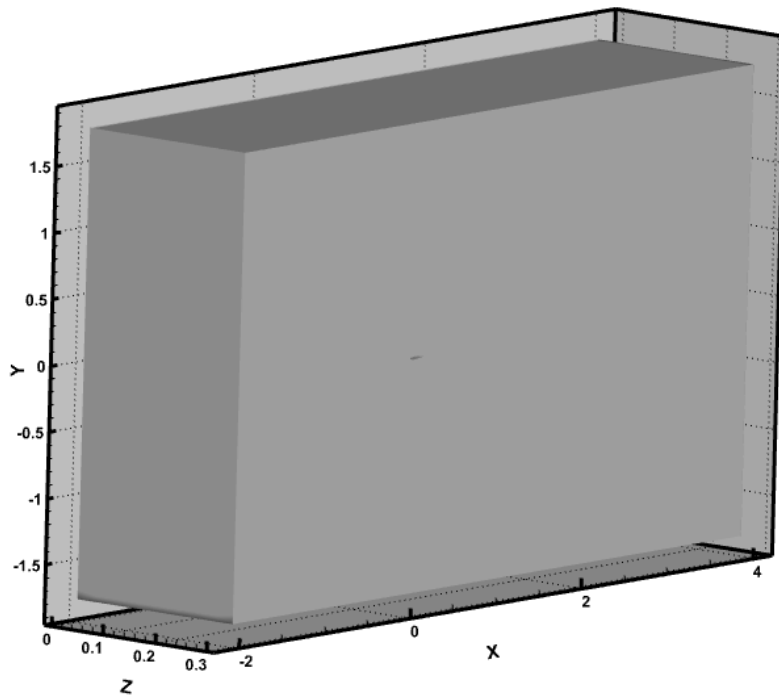


Fig. 3. Diagram of the domain used in the present work

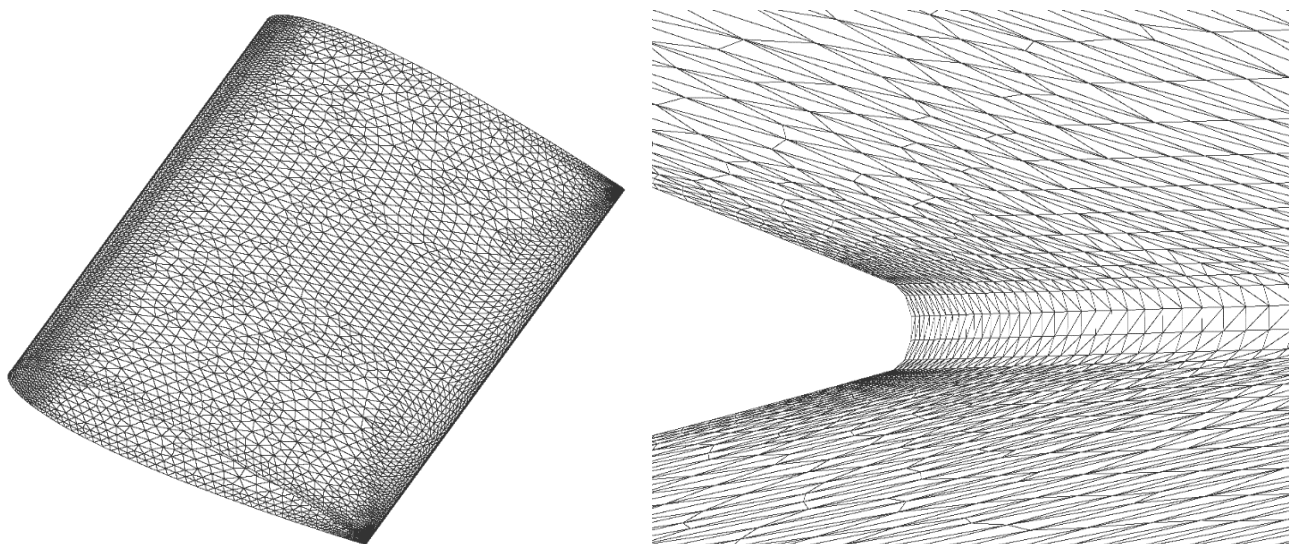


Fig. 4. Close-up view of the mesh over the airfoil's surface and at the trailing edge

3.3 Computational Set-up

Large-Eddy Simulation (LES) model is a type of numerical simulation that was utilized to examine the unsteady fluid flow within the computational domain. It is considered a more accurate and detailed approach than Reynolds-averaged Navier-Stokes (RANS) models as it resolves the large-scale, or "eddy," motions of the fluid. The LES model is particularly useful for simulating turbulent flows in complex geometries, such as those found on aircraft wing surfaces. The dynamic Smagorinsky model (DSM) is the method used to compute the sub-grid viscosity values in LES simulations. It calculates the Smagorinsky constant, which is used to model the sub-grid scale (SGS) viscosity, as a local value rather than using a single value for all cases as in the original Smagorinsky model. The local computation of the SGS viscosity allows the model to better capture the SGS dynamics near the wall, thus improving the accuracy of the results.

Simplec pressure-velocity integration scheme was employed, with gradients evaluated using the Green-Gauss node-based technique. To solve all equations, a second-order upwind discretization scheme was employed. To establish a suitable time-dependent solution formulation, a bounded second-order implicit method was chosen. The simulation was carried out using a fixed time-stepping scheme. After evaluating various time intervals, it was determined that a dimensionless time of 160, based on the free-stream velocity and airfoil chord, was sufficient for all cases. This was confirmed by examining both instantaneous and averaged lift (Cl) and Drag coefficients (Cd). The total simulation time was originally calculated using a method known as "hydraulic retention time." However, to ensure that the flow had sufficient time to traverse the domain twice, the estimated flow time was doubled. Furthermore, double precision was enabled in order to decrease the truncation error.

The airfoil surface was identified as the source of the acoustic wave, and four-receiver locations were chosen: one located upstream of the leading edge (8c), one above the suction side (8c), one below the pressure side (8c), and one downstream of the trailing edge (8c). All the observer positions were measured relative to the center of the airfoil. This distance is chosen for a balance between capturing relevant aerodynamic information and avoiding interference from immediate flow disturbances. At 8 chord lengths, the receivers are positioned sufficiently far from the airfoil surfaces to gather meaningful acoustic data representative of the overall flow behavior.

4. Comparison with other Study

4.1 Flow Characteristics

Several validations of the results have been carried out in the present study. Amongst useful resolution checks is comparing the present study's time-history lift coefficient with other studies [90]. The occurrence of periodic lift coefficients is a result of the transient behavior inherent in the flow dynamics. The cyclic variations in lift coefficients are indicative of the dynamic interaction between the airfoil and the surrounding fluid, reflecting the periodic changes in flow conditions over time. In comparison to a study with the same airfoil profile (NACA 0015) at a Reynolds number of about $R_e \approx 1.6 \times 10^5$ but slightly different bluntness at the trailing-edge, the time-history result of lift coefficients is shown in Figure 5. The airfoil bluntness used in this study is 1.5 mm, whereas the other study has a bluntness of about 1.3 mm. The lift coefficient time variations after convergence are seen with minor fluctuations in the present work and slightly higher fluctuations in the other study; the observed differences in the magnitude of oscillations might be due to the variation of airfoil bluntness or different numerical techniques used. However, they oscillate around a mean lift coefficient value

of about 0.43. The periodic lift coefficients occur because of vortices propagating through various regions on the airfoil surface, such as the unsteadiness within the wake locations.

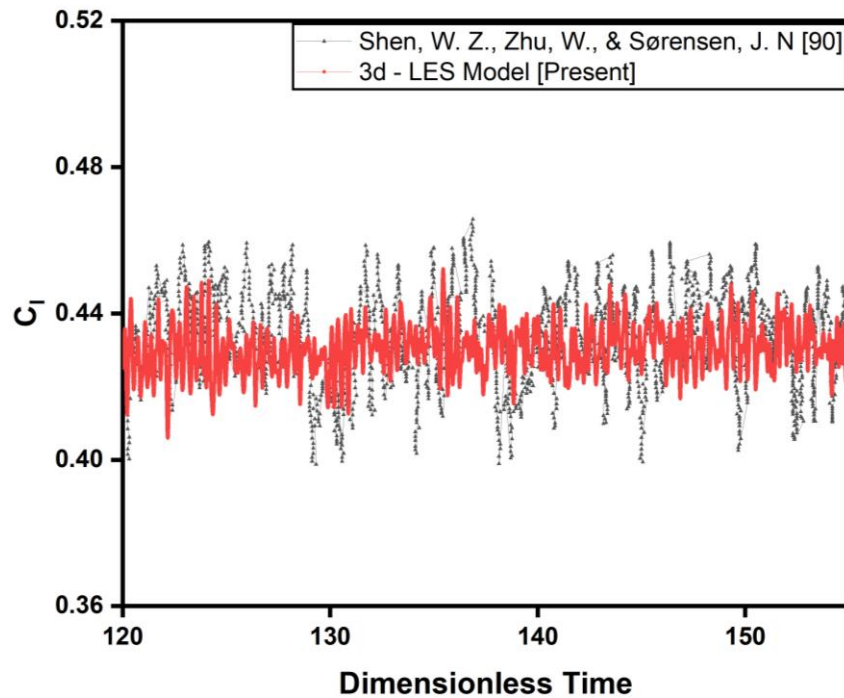


Fig. 5. Comparison of the present work with a numerical study

4.2 Surface Pressure Fluctuations

Comparing results from multiple simulations or observations is feasible by normalizing the pressure variations. These differences can result in the emission of sound, and the size of the pressure fluctuations can be used to anticipate the resulting noise levels. Therefore, it is vital to compare the normalized pressure fluctuations from the current research with those from another numerical result to identify noise levels appropriately.

A comprehensive assessment of the normalized pressure variations was carried out at specific locations within the flow domain. The fluctuation pattern presented on the normalised pressure fluctuation plot is related to another study [90]. As illustrated in Figure 6, the surface pressure signals computed using the present numerical model were examined at two points: one centred about 50% of the chord length on the suction side (90°) and another one upstream (0°). These locations are positioned $12c$ distant from the surface of the airfoil. The plot of the pressure variations at the suction side displays a unique pattern with a comparatively low amplitude of 0.00015 in contrast to a reference value. On the other hand, the changes on the upstream side are negligible since the reference pressure utilized is the ambient pressure of 101,325 Pa on the upstream side of the flow. The data reveal that the pressure differences are modest, proving the pressure measurements' accuracy. However, it is worth emphasizing that the significant purpose of this research is to compare the average pressure value between the present work and the numerical study. The mean value for the point placed on the suction side for both is roughly -0.00022, while for the upstream scenario, it is around 0.0001.

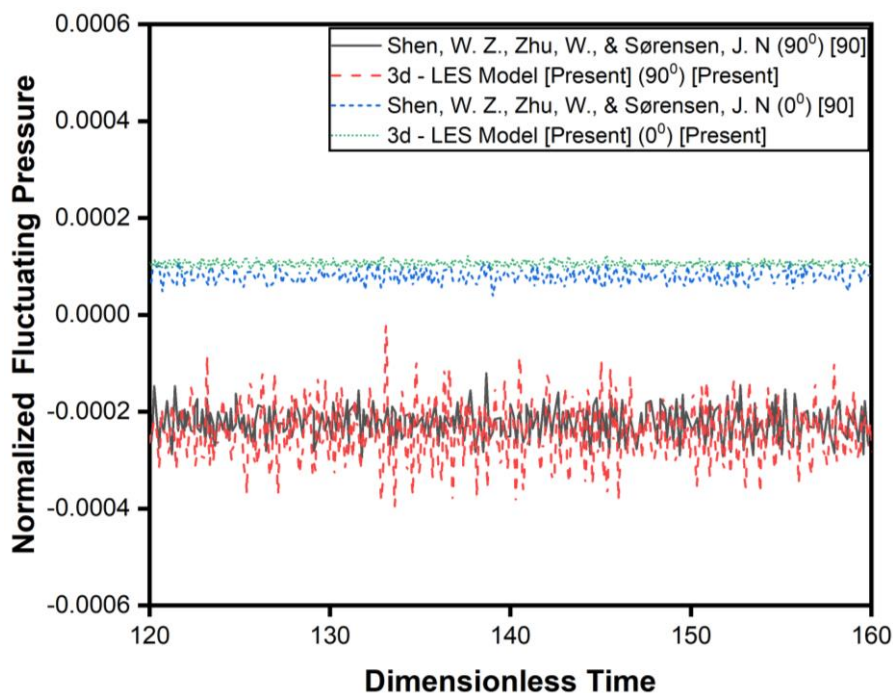


Fig. 6. Time histories of the normalized wall pressure at $\alpha = 4^\circ$

5. Far-Field Noise Prediction

5.1 Spectra of the Pressure Signal

In order to relate the spectral contents of signals, Figure 7 describes the results based on FFT analysis of several signals. This spectra offers valuable insights into the characteristics of pressure signals. The plot showcases prominent peaks at lower frequencies (< 103), which are identified as the characteristic frequencies. Additionally, the graph highlights the presence of a broadband spectrum at lower frequencies across all angles of attack, a pattern consistent among the different configurations examined. Notably, significant differences in the spectral shape are observed when considering various angles of attack, particularly between positive and negative angles of attack. However, these differences in the spectral shape are even more pronounced at high frequencies. Furthermore, it is observed that the baseline configuration exhibits a slightly higher frequency shift for the highest peak when compared to the other configurations. This suggests that the different configurations have varying effects on the power of the signal compared to the baseline. The baseline configuration generally yields a slightly higher magnitude within the lower frequency range, except for the combed trailing edge. These findings underscore the effectiveness of the serrated trailing-edge configuration in reducing noise across the entire frequency range. By adjusting the trailing-edge, researchers have the potential to enhance the noise performance of the wing.

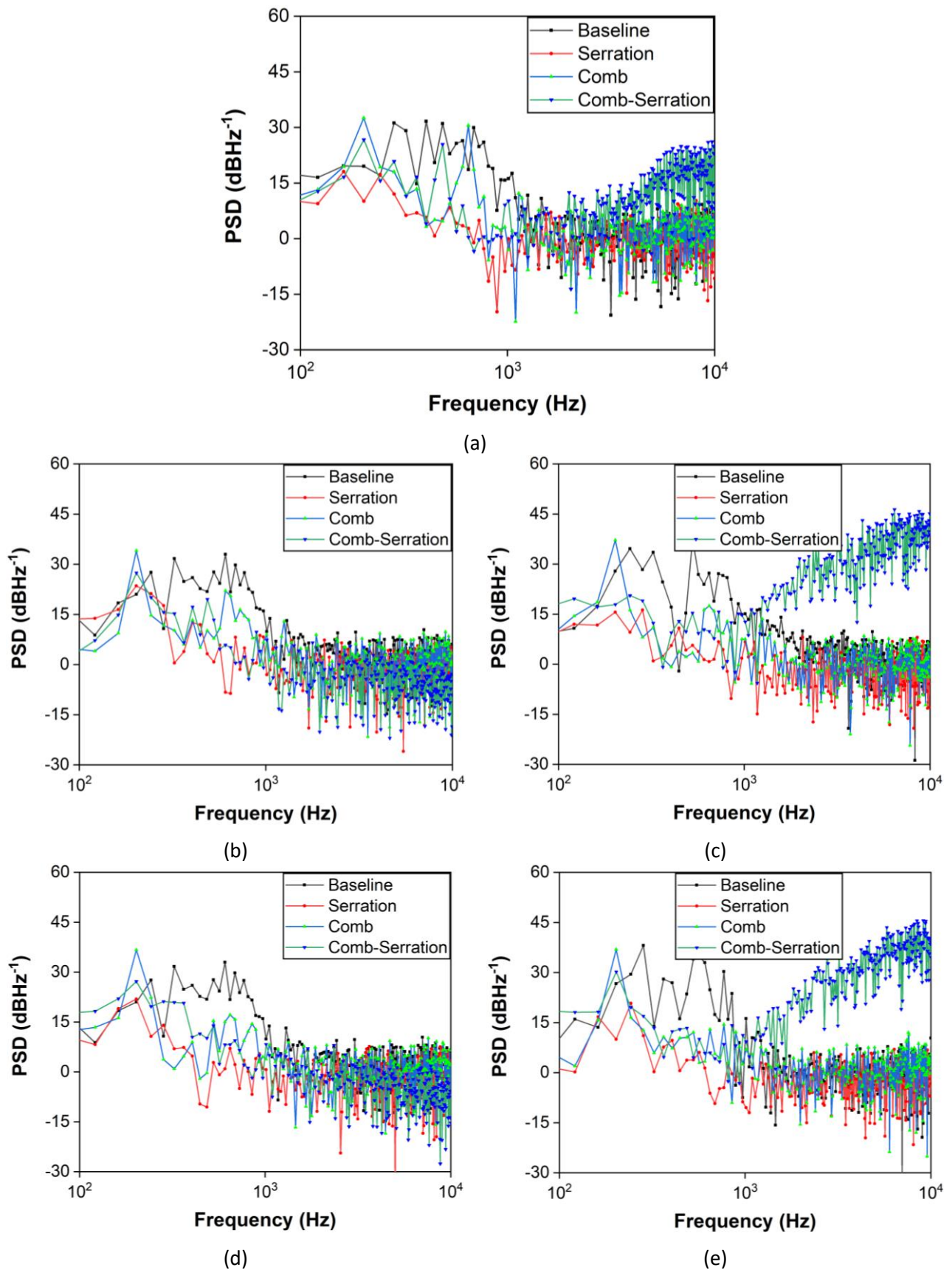


Fig. 7. PSD of Pressure Fluctuation at (a) $\alpha = 0^\circ$ (b) $\alpha = 1^\circ$ (c) $\alpha = -1^\circ$ (d) $\alpha = 2^\circ$ and (e) $\alpha = -2^\circ$

5.2 Sound Pressure Level

The Sound Pressure Level (SPL) is a crucial method for assessing the loudness of sounds in various environments. It offers a quantitative measurement of sound loudness and enables comparisons between different sounds. Sound pressure level can also be employed to evaluate the efficiency of noise reduction techniques such as trailing edge configurations. The results of the SPL analysis can be used to identify noise sources and develop strategies for reducing noise levels. Moreover, SPL analysis can also be used to evaluate the compliance of a particular technique with regulations and standards related to noise pollution.

In this investigation, the acoustic field was computed using the Ffowcs, Williams, and Hawkings model based on the unsteady aerodynamic flow field acquired from large-eddy simulation. The whole surface of the airfoil has been selected as the source of the radiated signals because it provides a comprehensive understanding of the noise created around the airfoil's surface. For this study, the acoustic receivers were strategically placed 8 chord lengths apart from the top (90°), and bottom (270°) surfaces as well as downstream (180°) of the flow. This location facilitates the prediction of pure acoustic signals as less fluctuation is encountered further away from the surfaces. By monitoring the sound pressure level at these different points, it can discover which parts of the airfoil are the primary producers of noise and how the noise is spread throughout the whole surface of the airfoil. Overall, this strategic arrangement of the receivers provides a thorough understanding of the noise-generating process and its dispersion. The observers are positioned on the mid-span plane of the airfoil since it is an optimal place for recording the noise emitted by the airfoil. In addition, acoustic signals were acquired at every time step, equivalent to a sampling frequency of 20 kHz. This permits the detection of sound pressure levels up to a maximum frequency of 10 kHz, which is suited for the current analysis as it focuses on low-frequency noise analysis.

The study gives sound pressure level (SPL) as the primary measure to quantify and compare noise sources at different angles of attack ($-2 \leq \alpha \leq 2^\circ$). By calculating the Fast Fourier Transform (FFT) on the wall pressure signals at the four observer locations, the third-octave sound pressure level as a function of frequency is produced and depicted in Figures 8, Figure 9, and Figure 10. The figures demonstrate how the SPL fluctuates with frequency, demonstrating which frequencies contribute more to the overall noise level. Based on Figure 8, the graph shows the noise level as a function of frequency for various trailing edge configurations of the airfoil. The trend of the noise level for the baseline configuration demonstrates that the noise level increases dramatically at lower frequencies and afterward diminishes towards the higher frequencies. This pattern is consistent across all the angles of attack indicated on the graph. The fact that the noise level is greater at lower frequencies shows that the noise source creates more low-frequency noise, consistent with prior research at low to moderate Reynolds numbers [86]. When comparing the trend of the noise level for the serrated design to that of the baseline configuration, it can be observed that there is a drop in the noise level over the entire frequency range displayed on the graph. This decrease is more noticeable at frequencies below 1.6 kHz, where the decrease is roughly 21 dB, therefore demonstrating that the serrated structure is more successful in suppressing low-frequency noise. Similarly, the trend of the noise level for the comb design indicates a reduction of about 14 dB in the low-frequency noise level compared to the baseline configuration, although the drop is not as large as that of the serration configuration. Finally, the SPL frequency analysis for the comb-serration arrangement demonstrates a reduction in low-frequency noise levels and an increase in high-frequency noise levels in most situations. The comb-serration model demonstrates a substantial increase of approximately 17 dB in the high-frequency range for angles of attack at 0, -1, and -2 degrees. However, as compared to the baseline configuration, the comb-serration arrangement displays the best reduction in high-

frequency noise levels at attack angles of 1 degree and 2 degrees, achieving a reduction of approximately 9 dB.

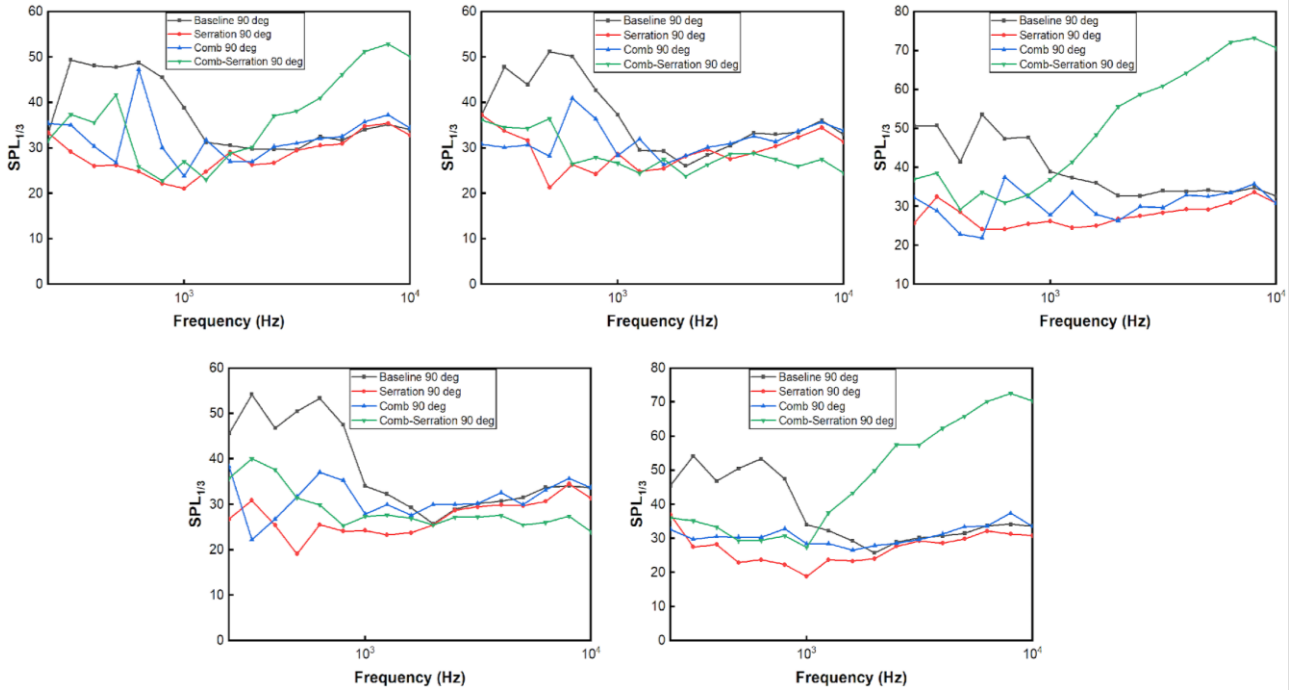


Fig. 8. Sound pressure level as a function of frequency at the suction side (a) $\alpha = 0^\circ$ (b) $\alpha = 1^\circ$ (c) $\alpha = -1^\circ$ (d) $\alpha = 2^\circ$ and (e) $\alpha = -2^\circ$

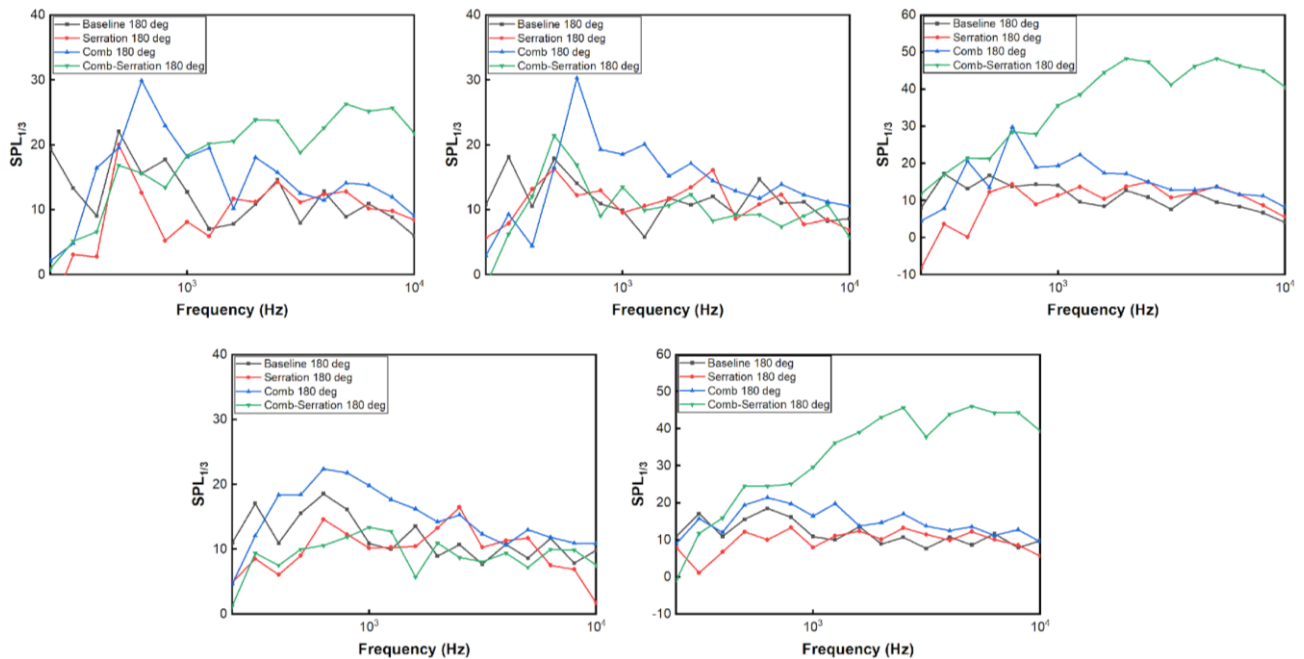


Fig. 9. Sound pressure level as a function of frequency at the wake region (a) $\alpha = 0^\circ$ (b) $\alpha = 1^\circ$ (c) $\alpha = -1^\circ$ (d) $\alpha = 2^\circ$ and (e) $\alpha = -2^\circ$

The graph in Figure 9 displays the sound pressure level as a function of frequency for various trailing edge designs of the airfoil in the wake region. The examination of the sound pressure level trend for the baseline configuration suggests a little rise in noise level at lower frequencies, followed by a slight drop at higher frequencies. This pattern is consistent across all angles of attack displayed

on the graph, showing that the noise source is emitting a combination of both low and high frequency noise. Upon inspection of the sound pressure level trend for the serrated design in reference to the baseline configuration, it can be noticed that the noise levels are fairly consistent over the frequency range, except for a small difference at the lower end of the frequency spectrum. This pattern illustrates that serration does have a significant impact on the acoustic level in the wake zone. The measurement of the sound pressure level trend for the comb design indicates a high noise level across most of the frequency range when compared to the baseline configuration. On the other hand, the SPL trend for the comb-serration design demonstrates an overall reduction in noise levels across the frequency range, notably at angles of attack of 1 and 2 degrees, when compared to the baseline configuration. Moreover, the comb-serration model demonstrates a substantial increase of approximately 17 dB in the high-frequency range for angles of attack at 0, -1, and -2 degrees.

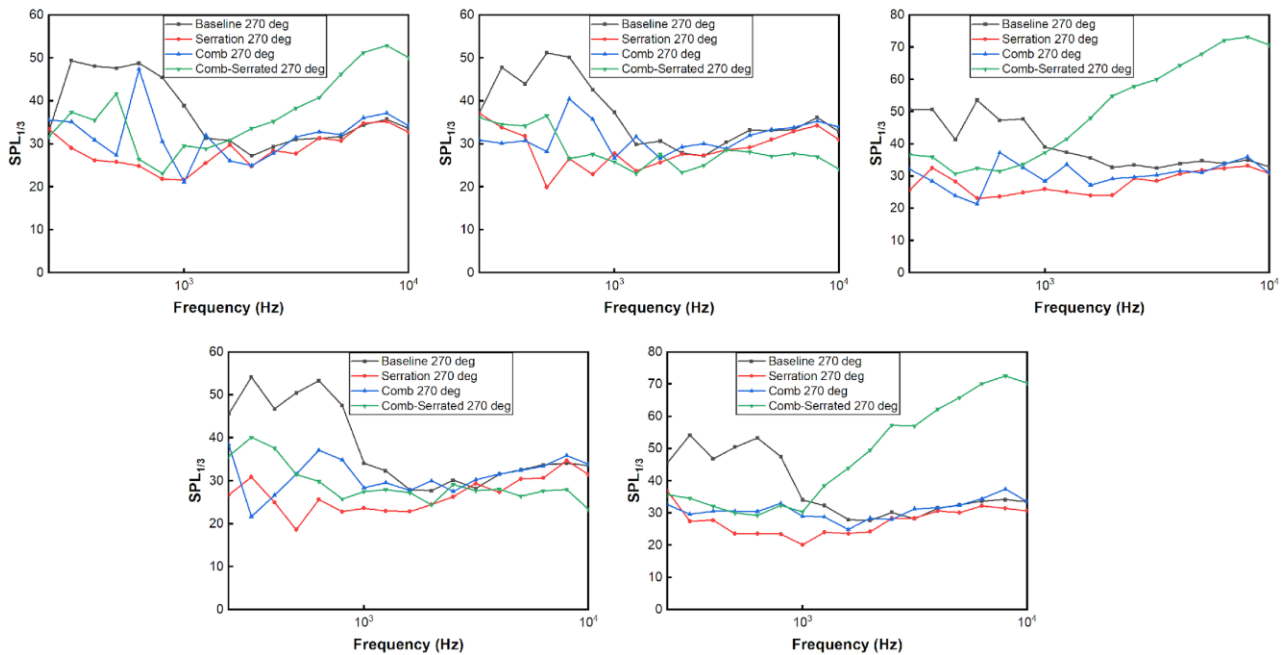


Fig. 10. Sound pressure level as a function of frequency at the pressure side (a) $\alpha = 0^\circ$ (b) $\alpha = 1^\circ$ (c) $\alpha = -1^\circ$ (d) $\alpha = 2^\circ$ and (e) $\alpha = -2^\circ$

The graph given in Figure 10 illustrates the sound pressure level as a function of frequency for various trailing edge configurations of the airfoil. The trend of the noise level for the baseline design indicates that the noise level increases dramatically at lower frequencies and gradually drops as the frequency increases on the pressure side. This pattern is consistent across all the angles of attack displayed on the graph and implies that the noise source is emitting more low-frequency noise. A similar pattern is seen on the suction side of the airfoil surface. When evaluating the trend of the noise level for the serration configuration in comparison to the baseline configuration on the pressure side, it can be noted that there is a drop in the noise level across the entire frequency range displayed on the graph. This decline is particularly noticeable at frequencies below 1.6 kHz, showing that the serrated arrangement is more efficient in decreasing low-frequency noise on the pressure side too. Similarly, the trend of the noise level for the comb configuration also reveals a reduction in low-frequency noise level compared to the baseline design on the pressure side; however, the drop is not as large as that of the serration configuration. Finally, the study for the comb-serration design on the pressure side indicates a reduction in low-frequency noise levels; nevertheless, an increase in high-frequency noise levels is noted in most situations. Nevertheless, as compared to the baseline

configuration on the pressure side, the comb-serration design still displays an overall reduction in high-frequency noise levels at angles of attack of 1 degree and 2 degrees. This shows that the comb-serration design is successful in decreasing noise levels on the pressure side in the low-frequency region while still offering some amount of noise reduction in the high-frequency range for a specified range of angles of attack.

5.3 Peak Noise Level and Primary Frequency

The peak noise level provides information on the highest sound intensity at a certain instant or location, whereas the average noise level offers a better representation of the total noise exposure over a prolonged period of time, often measured in decibels (dB). In the current research, these data are especially valuable for determining the possible influence of various models on the suction, pressure, and wake region. The trend of the maximum sound pressure level as a function of angle of attack for different trailing edge designs of the airfoil is depicted in Figure 11. The baseline configuration displays a steady rise in SPL with increasing attack angle, reaching a peak at 2 degrees. This pattern indicates that as the angle of attack increases, so does the degree of noise emitted by the airfoil surfaces. Notably, it is found that the noise level does not reflect symmetry with regard to the aerodynamic characteristics when comparing negative and positive angles of attack, except for 2 degrees. When comparing the serration configuration to the baseline configuration, it can be noted that there is a rise in the peak SPL throughout the entire range of angles of attack given on the graph, with the exception of -2 degrees to -1 degree. The greatest peak SPL of 39.6 dB is seen at around 1 degree, and a little drop is found at 2 degrees, demonstrating that the serrated trailing edge is more successful in suppressing noise levels. Similarly, the pattern of the highest SPL for the comb arrangement shows a decline until 0 degrees and then a steady rise until 2 degrees, with a maximum peak SPL of around 53 dB. In contrast, the comb-serration design displays a drop in the maximum SPL as the angle of attack increases, with the exception of -2 degrees to -1 degree. The maximum peak SPL of 73 dB is observed at -1 degree. These findings indicate the noise reduction capabilities of the comb-serration and serration configurations at different angles of attack.

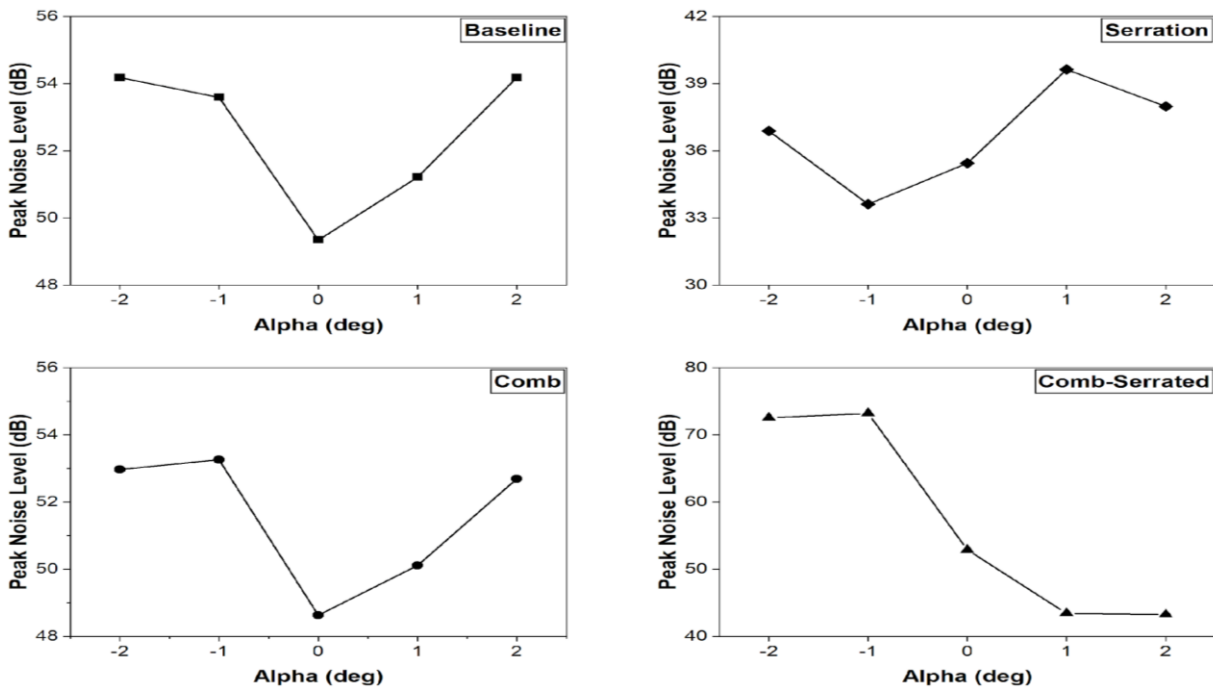


Fig. 11. The maximum noise level recorded at different angles of attack on the suction side of the airfoil

The maximum sound pressure level graph (Figure 12) displays varied trailing edge designs in the wake zone. The baseline design demonstrates a variation in SPL, with a fall until -1 degree, an increase up to 0 degree, and then a decrease thereafter. This pattern implies that when the angle of attack rises, the degree of noise created by the airfoil surfaces changes at the wake area. Additionally, it is found that the noise level does not display a clear pattern of symmetry when comparing negative and positive angles of attack. However, the serrated trailing edge presents an overall rise in noise level until 0 degrees, followed by a drop. This suggests that the serrated trailing-edge is less successful in decreasing noise levels in the wake region when the angle of attack is raised to 2 degrees. A comb structure displays an increase in SPL until -1 degree and then a continuous rise until 1 degree, followed by a reduction again. Lastly, the comb-serration reveals a similar trend to that found on the suction side, with a drop in peak noise level as the angle of attack increases. Moreover, a serrated trailing edge indicates the possibility of lowering noise level at a low angle of attack, but a comb-serrated trailing edge illustrates its potential at a high angle of attack.

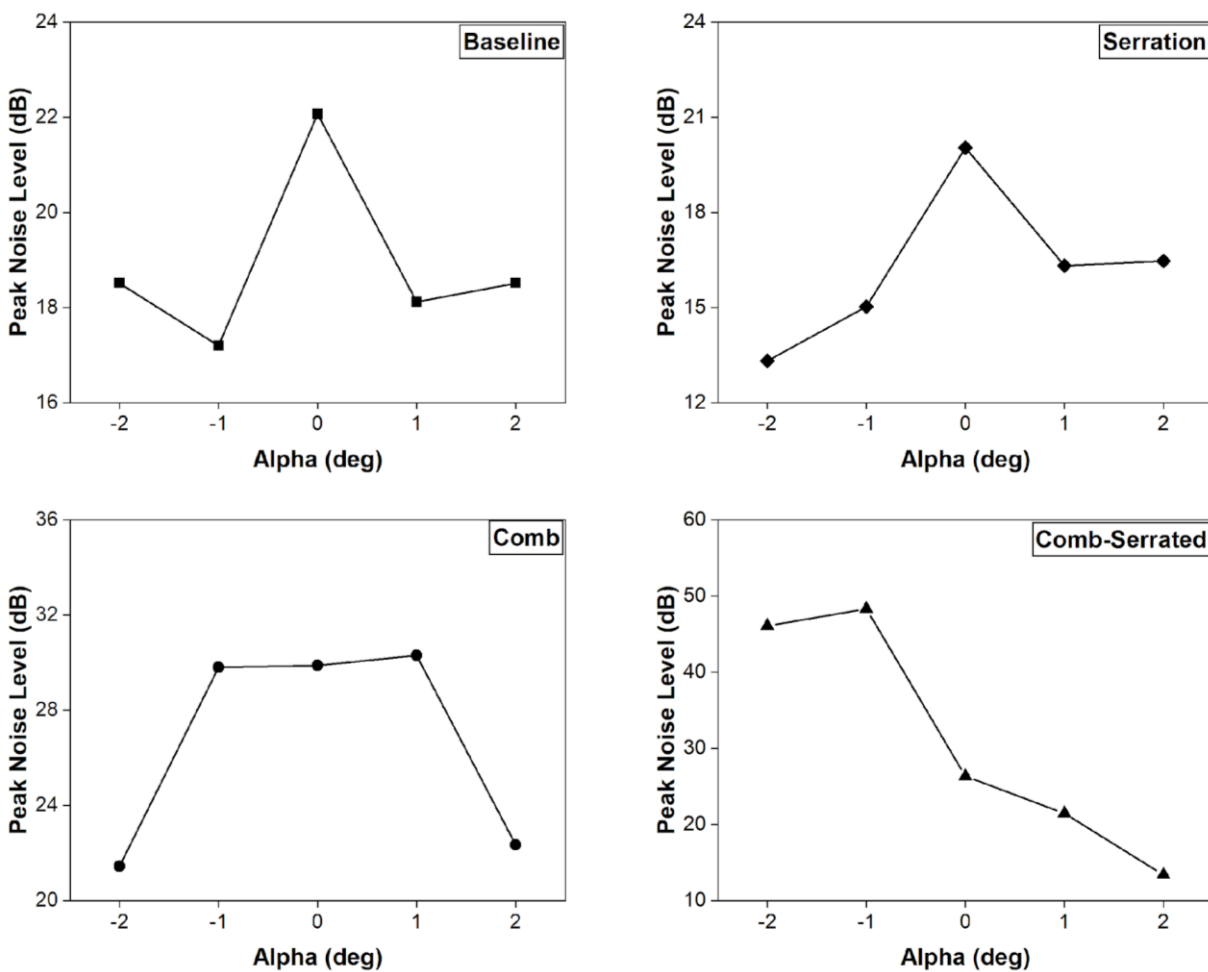


Fig. 12. The maximum noise level recorded at different angles of attack at the wake region of the airfoil

Figure 13 shows the fluctuation of the peak sound pressure level in proportion to the angle of incidence for various trailing edge designs. Clearly, it can be seen that the baseline configuration demonstrates a gradual increase in the peak level as the angle of attack is increased from 0 degrees to 2 degrees, indicating that the noise level generated by the airfoil surfaces increases as the angle of attack increases, consistent with the trend observed on the suction side. Additionally, symmetry is exhibited only at 2 degrees, and the noise level does not demonstrate symmetry in reference to

the aerodynamic parameters when comparing negative and positive angles of attack. The serration structure similarly demonstrates an increase in the peak noise level throughout most of the angles of attack indicated in the graph, with the highest peak noise level seen at 1 degree. A similar trend is apparent for the comb trailing edge, with a drop in the noise level until 0 degrees and then a progressive increase until 2 degrees, with a maximum peak SPL of roughly 53 dB when measured at the pressure side. Moreover, the comb-serration design similarly showed a decline in the greatest noise level as the angle of attack increases, with the highest peak noise level of 73 dB measured at a -1 degree angle. Overall, these results also demonstrate the possibility for noise reduction when utilizing comb-serration and serration geometries at varied angles of attack.

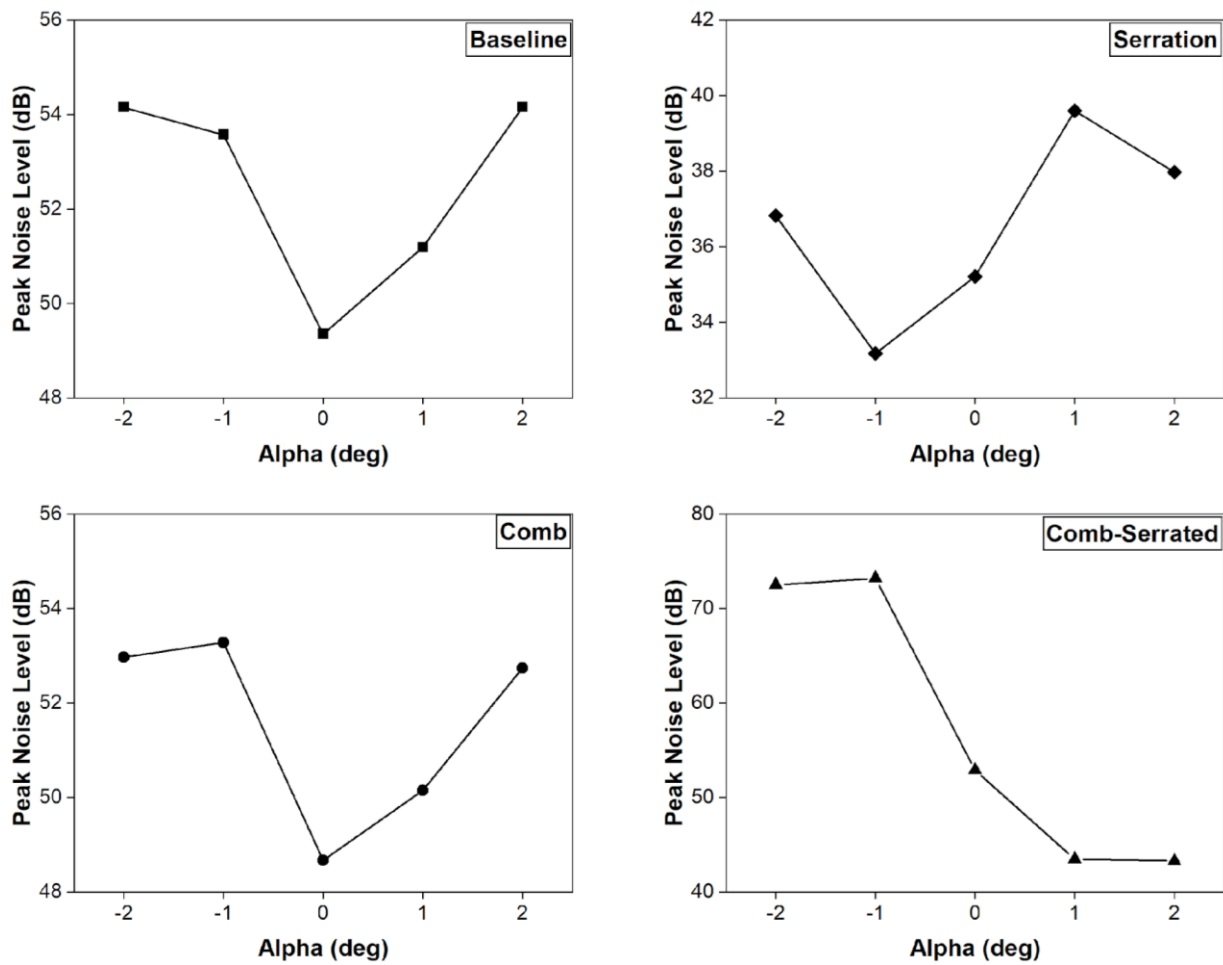


Fig. 13. The maximum noise level recorded at different angles of attack on the pressure side of the airfoil

The peak frequency of a sound signal is defined as the frequency at which the sound pressure level or acoustic energy density is greatest. Researchers can identify the dominant sound-producing mechanism or flow characteristic of an aerodynamic system by evaluating the peak frequency. In the case of airfoil noise, for example, the peak frequency is associated with the unsteady flow characteristics around the airfoil. Understanding the connection between the peak frequency and the underlying flow characteristics allows researchers to devise ways for mitigating or controlling sound emission and improving the system's overall acoustic performance. The graph in Figure 14 depicts the trend of the peak frequency as a function of the angle of attack for various trailing edge configurations of the airfoil on the suction side. The baseline design demonstrates a variation in peak frequency as the angle of attack increases, with an initial increase from -2 degrees to -1 degrees, followed by a reduction up to 0 degrees, an increase up to 1 degree, and then a decrease again. This

pattern implies that when the angle of attack increases, the peak frequency of the noise created by the airfoil surfaces goes to higher frequencies and then returns to lower frequencies. Furthermore, it is noticed that the peak frequency displays asymmetric behaviour in respect to the aerodynamic parameters when comparing negative and positive angles of attack, unlike the peak noise level plot. When evaluating the trend of the peak frequency for the serration configuration in comparison to the baseline configuration, it can be noted that there is an increase in the peak frequency from -2 degrees to 0 degrees, followed by a reduction thereafter. This illustrates that the serrated trailing edge moves the main frequency towards lower frequencies as the angle of attack rises until 2 degrees and has minimal influence on the peak frequency between 1 degree and 2 degrees. The trend of the peak frequency for the comb design exhibits little fluctuation as the angle of attack increases, showing that it has little influence on shifting the main frequency. Finally, the peak frequency analysis for the comb-serration arrangement reveals a similar pattern at low angles of attack and a reduction in peak frequency at high angles of attack. This suggests that the comb-serration design is successful in shifting the peak frequency to lower frequencies at high angles of attack and has minimal effect at low angles of attack.

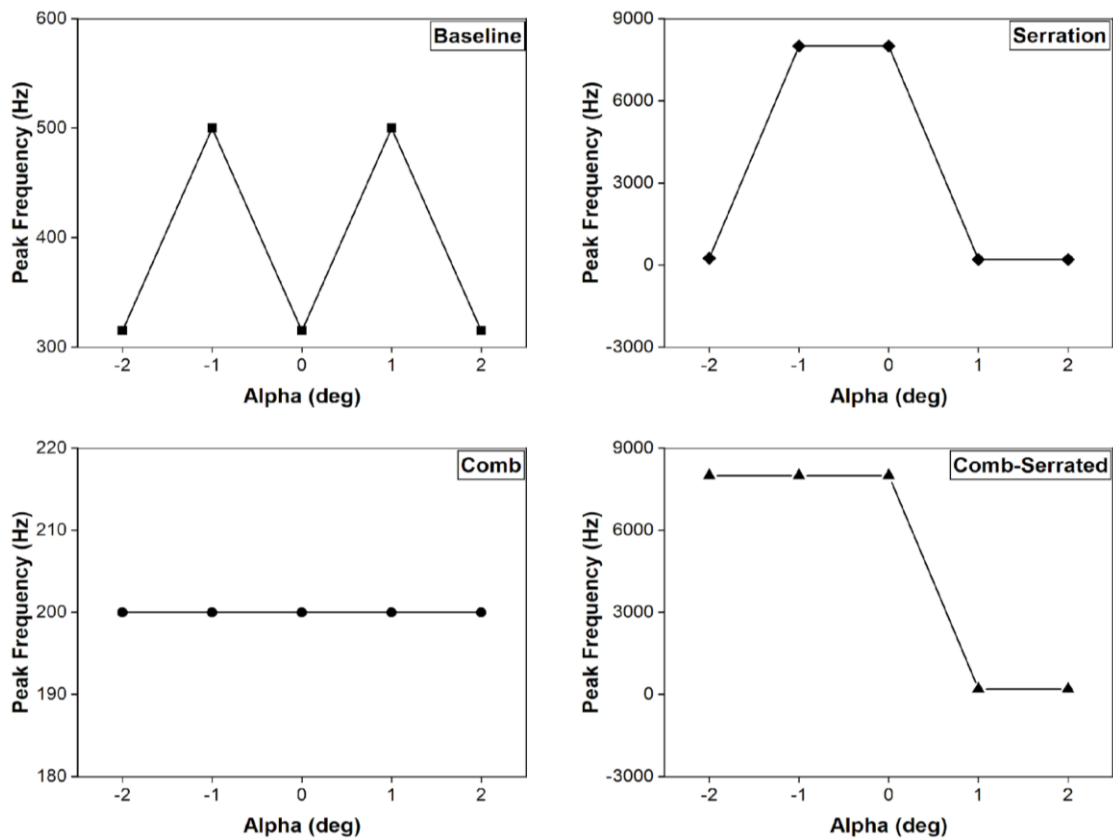


Fig. 14. The frequency of the highest noise level on the suction side for various angles of attack

The study of the peak frequency as a function of the angle of attack for various trailing edge configurations of the airfoil in the wake area is provided in Figure 15. The baseline setup demonstrates a variation in the peak frequency when the angle of attack is varied, described by an initial drop from -2 degrees to -1 degrees, followed by an increase up to 0 degrees, a decrease up to 1 degree, and then an increase again. This pattern implies that when the angle of attack increases, the peak frequency of the noise created by the airfoil surfaces falls to lower frequencies and then returns to higher frequencies. Furthermore, it is also seen that the peak frequency displays asymmetric behaviour in respect to the aerodynamic parameters when comparing negative and

positive angles of attack, unlike the peak noise level plot. Regarding the serration arrangement, it can be noted that there is a rise in the peak frequency from -2 degrees to -1 degree, followed by a reduction up to 0 degree and then an increase thereafter. This indicates that the serrated trailing edge shifts the main frequency towards higher frequencies as the angle of attack increases from 0 degrees to 2 degrees, with no influence on the peak frequency between 0° and 1°. Like the suction side, the trend of the peak frequency for the comb design displays little fluctuation when the angle of attack increases, showing that it has little influence on shifting the main frequency. The peak frequency study for the comb-serration arrangement likewise reveals a stable trend at low angles of attack and a reduction in peak frequency at high angles of attack, which is consistent with the suction side. Thus, it can be extrapolated that the comb-serration design is successful in shifting the peak frequency to lower frequencies at high angles of attack but has minimal impact at low angles of attack.

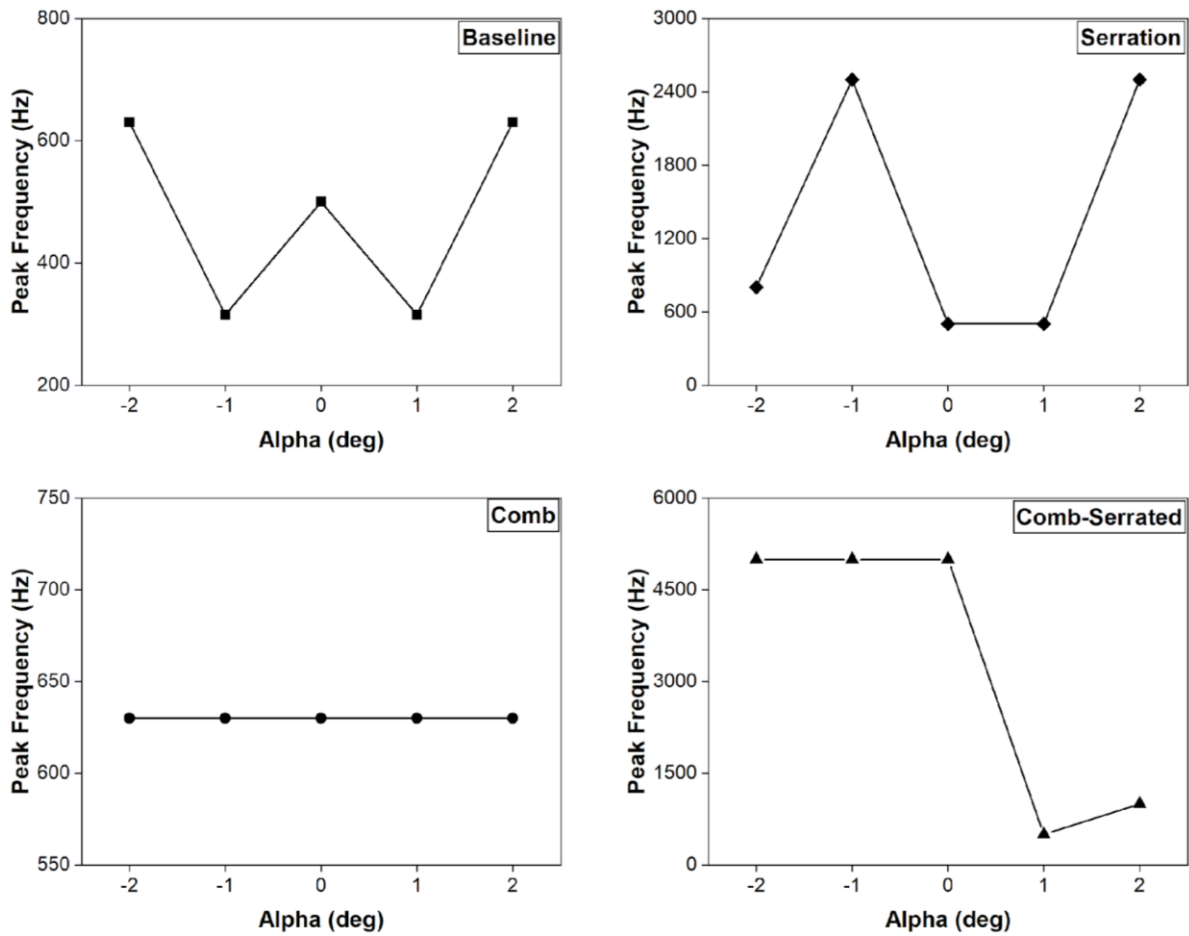


Fig. 15. The frequency of the highest noise level at the wake region for various angles of attack

The graph in Figure 16 demonstrates the trend of the peak frequency as a function of angle of attack for various trailing edge configurations of the airfoil on the pressure side. The trends found in this graph are comparable with those reported on the suction side, where similar oscillations in peak frequency are exhibited. The baseline arrangement illustrates that when the angle of attack increases, the peak frequency of the noise created by the airfoil surfaces goes to higher frequencies and then returns to a lower frequency. Additionally, it is also noted that the peak frequency displays a symmetric pattern. Similarly, the serrated trailing-edge also indicated the shift of the main frequency towards lower frequencies when the angle of attack is raised until 2 degrees and no

influence on the peak frequency between 1 degree and 2 degrees. Moreover, the comb configuration shows little variability when the angle of attack varies, indicating that it has little influence on the shifting of the main frequency. Lastly, the comb-serration design also confirmed its effectiveness in shifting the primary frequency to a lower frequency at high angles of attack and having less effect at low angles of attack. This illustrates the uniformity of the results and the effectiveness of the comb-serration arrangement in decreasing noise levels on the pressure side as well as the suction side.

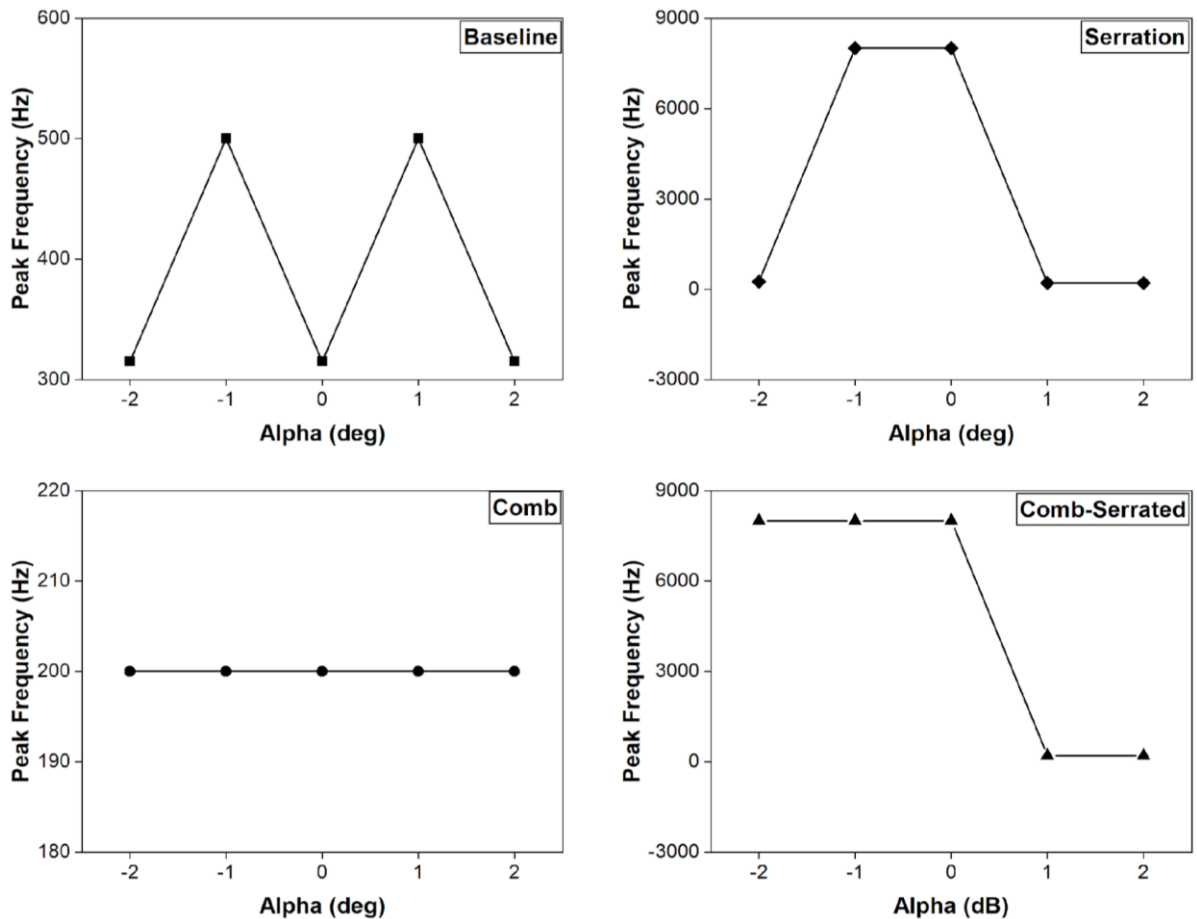


Fig. 16. The frequency of the highest noise level on the pressure side for various angles of attack

5.4 Directivity Pattern

The directivity pattern of an acoustic source defines the directionality of the radiated sound field emitting from the acoustic source. In addition, it also elaborates on the direction with the highest radiated sound pressure, which assists in pointing out the area of concern. The noise directivity pattern at different angles of attack is often represented by a polar plot, such as that shown in Figure 17. From the graph, it can be noted that the directivity pattern of the source is extremely directional, with the maximum overall sound level in the direction of 90 degrees and 270 degrees and a minimum level in the direction of 0 degrees and 180 degrees. This pattern is consistent across all models, showing that most of the source's acoustic energy is being emitted in the direction of 90 degrees and 270 degrees and comparatively less energy in the direction of 0 degrees and 180 degrees. This also confirms the necessity of monitoring the noise level on the suction and pressure sides of the airfoil surfaces. Additionally, the directivity pattern reveals a relatively symmetric structure, with a comparable sound pressure level in the directions of 90 and 270 degrees, suggesting that the source is producing energy in a relatively consistent manner in those directions. However, the effect of

angles of attack is inconsistent across different configurations. For the baseline, the figure indicates a considerable rise in the noise level when the angle of attack is raised from 0 degrees to 2 degrees in the region below the airfoil surface. On the suction side, an increase is noted exclusively from 0 to 1 degree with an almost comparable noise level at 2 degrees. On the other hand, upstream and downstream sides exhibit a consistent level of noise across the angles of attack, with a little increase in the upstream direction at 2 deg. The overall noise level rose by roughly 6 dB and 5 dB as the angle of attack increased from 0 to 1 degree for the suction and pressure sides, respectively. However, a difference of roughly 9 dB and 19 dB is detected as the angle of attack increases further to 2 degrees. The serrated trailing-edge resulted in a greater noise level as the angle of attack increased from 0 to 2 degrees on the suction and pressure sides; however, a drop in the noise level was seen in the upstream and downstream directions. Furthermore, the comb model predicts a decrease in the overall noise level as the angle of attack is increased to 1 degree, followed by an increase when the angle of attack is increased to 2 degrees on the suction and pressure sides. Both the wake region and upstream side resulted in noise reduction throughout the angles of attack. Nonetheless, the comb-serrated design provided a dramatic drop in the total noise level as the attack angle rose to 2 degrees. Notably, the complete structure of the noise pattern is not reflected effectively as we employed only four observer positions, but significantly more spots around the airfoil surface are necessary.

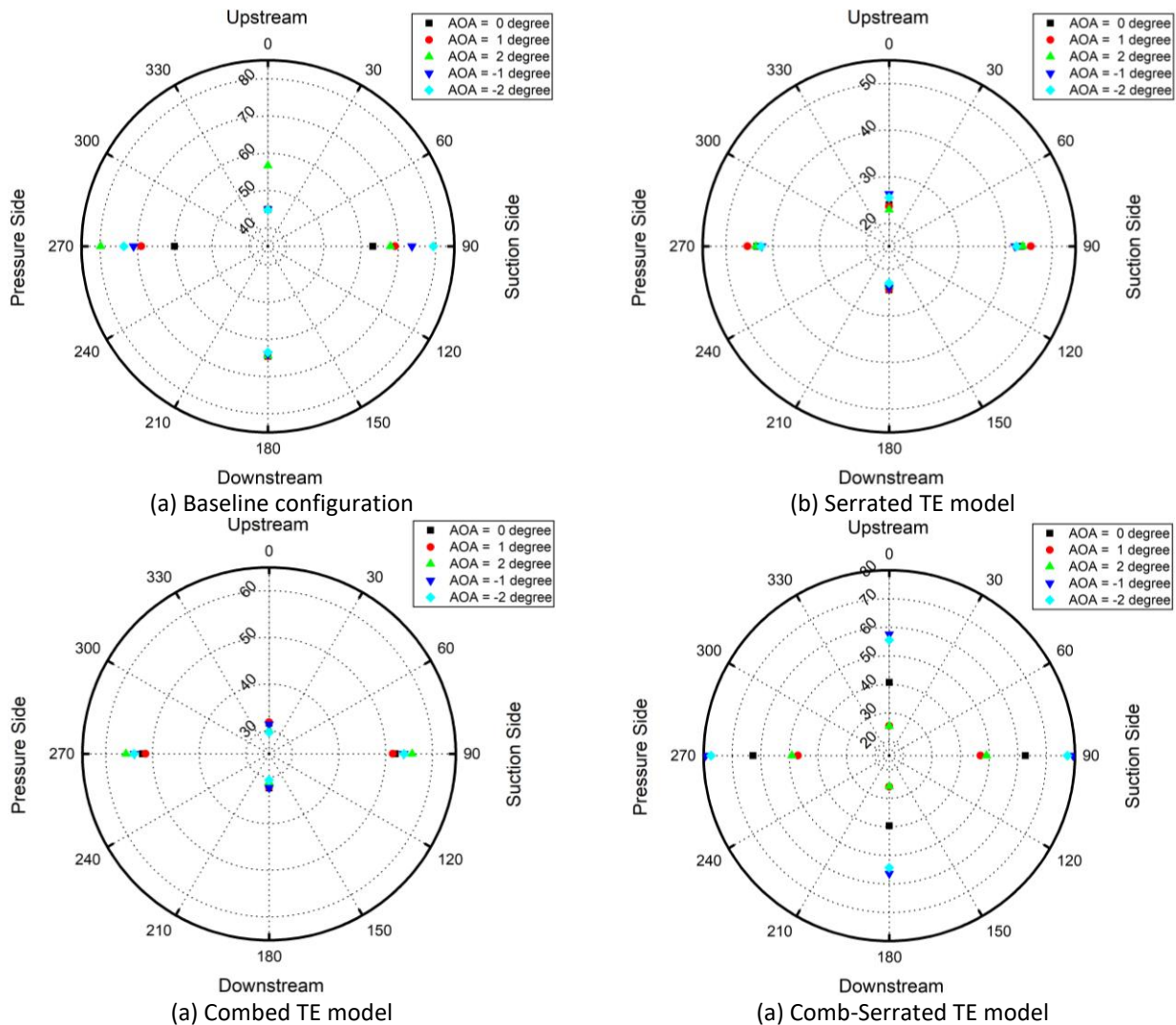


Fig. 17. The directivity of the acoustic signals measured at a radial distance of 12 chords from the airfoil center

6. Conclusions

The present findings were analyzed through large-eddy simulation conducted on a NACA0015 airfoil, investigating four different types of trailing edges (baseline, comb, serrated and comb-serrated) at a low Reynolds number of 1.6×10^5 . The radiated noise was predicted using the Ffowcs-Williams and Hawkings model. The numerical model demonstrates its effectiveness in accurately capturing the fluctuations in the lift coefficient and pressure measurements when compared to a previously published study. However, the observed discrepancies in the amplitude of oscillations might be attributable to the changes in airfoil bluntness or different numerical approaches applied. This analysis also demonstrated that the lift coefficient pattern is consistently accurate across all angles of attack. Based on the spectra of the pressure signal, prominent peaks at lower frequencies ($< 10^3$) are observed, which are identified as the characteristic frequencies. Furthermore, the results also showcase an irregular broadband spectrum with a center frequency of roughly 300–600 Hz for all cases. The noise levels for the baseline are seen higher at lower frequencies, suggesting that the source is emitting low-frequency noise. However, the Serrated trailing edge model indicated a drop in the noise level over the whole frequency range and was more noticeable at lower frequencies below 1.6 kHz, where the decrease is roughly 21 dB, therefore showing that this design is more successful in decreasing low-frequency noise. Additionally, the combed trailing edge exhibited a slight reduction in the noise level at low frequencies. Contrarily, the comb-serration model demonstrates a substantial increase of approximately 17 dB in the high-frequency range for angles of attack at 0, -1, and -2 degrees. However, as compared to the baseline configuration, the comb-serration arrangement displays the best reduction in high-frequency noise levels at attack angles of 1 degree and 2 degrees, achieving a reduction of approximately 9 dB. This study implies that serration and comb-serration are key in reducing noise at high angles of attack. On the other hand, the directivity pattern showed that the maximum noise level is observed to predominantly radiate at an azimuth angle of around 90 degrees for all the cases, ranging from 90 to 270 degrees, indicating that the majority of the source's acoustic energy is being emitted on the suction and pressure sides of the wing. These findings imply that the broadband noise is highly dependent on the angle of attack, not only on noise level but also on the directivity pattern.

Acknowledgement

This research was supported by the Ministry of Education (MOE) through Fundamental Research Grant Scheme (FRGS/1/2018/TK09/UIAM/03/4). We would also like to thank IIUM for financial support under the KOE Postgraduate Tuition Fee Waiver Scheme 2019 (TFW2019).

References

- [1] Roslan, Siti Amni Husna, Zainudin A. Rasid, and Ahmad Kamal Ariffin. "Extended blade element momentum theory for the design of small-scale wind turbines." *Journal of Advanced Research in Applied Mechanics* 101, no. 1 (2023): 62-75. <https://doi.org/10.37934/aram.101.1.6275>
- [2] Celik, Alper, J. Luke Bowen, and Mahdi Azarpeyvand. "Effect of trailing-edge bevel on the aeroacoustics of a flat-plate." *Physics of Fluids* 32, no. 10 (2020). <https://doi.org/10.1063/5.0024248>
- [3] Wang, Lei, Xiaomin Liu, and Dian Li. "Noise reduction mechanism of airfoils with leading-edge serrations and surface ridges inspired by owl wings." *Physics of Fluids* 33, no. 1 (2021). <https://doi.org/10.1063/5.0035544>
- [4] Chong, Tze Pei, and Elisa Dubois. "Optimization of the poro-serrated trailing edges for airfoil broadband noise reduction." *The Journal of the Acoustical Society of America* 140, no. 2 (2016): 1361-1373. <https://doi.org/10.1121/1.4961362>
- [5] Vemuri, S. H., Xiao Liu, B. Zang, and Mahdi Azarpeyvand. "On the use of leading-edge serrations for noise control in a tandem airfoil configuration." *Physics of Fluids* 32, no. 7 (2020). <https://doi.org/10.1063/5.0012958>

- [6] Ramli, Muhammad Ridzwan, Wan Mazlina Wan Mohamed, Hamid Yusoff, Mohd Azmi Ismail, Ahmed Awaludeen Mansor, Azmi Hussin, and Aliff Farhan Mohd Yamin. "The Aerodynamic Characteristics Investigation on NACA 0012 Airfoil with Owl's Wing Serrations for Future Air Vehicle." *Journal of Advanced Research in Fluid Mechanics and Thermal Sciences* 102, no. 1 (2023): 171-183. <https://doi.org/10.37934/arfmts.102.1.171183>
- [7] Jefferies, R. "Continuous Lower Energy, Emissions and Noise (CLEEN) Program." In *USACA Spring Association Meeting, 21 May*. 2013.
- [8] Dobrzynski, Werner. "Almost 40 years of airframe noise research: what did we achieve?." *Journal of aircraft* 47, no. 2 (2010): 353-367. <https://doi.org/10.2514/1.44457>
- [9] Kallas, Siim, Máire Geoghegan-Quinn, M. Darecki, C. Edelstenne, T. Enders, E. Fernandez, and P. Hartman. "Flightpath 2050 Europe's vision for aviation." *Report of the high level group on aviation research, European commission, Brussels, Belgium, Report No. EUR 98*. 2011.
- [10] Camussi, Roberto, and Gareth J. Bennett. "Aeroacoustics research in Europe: The CEAS-ASC report on 2019 highlights." *Journal of Sound and Vibration* 484 (2020): 115540. <https://doi.org/10.1016/j.jsv.2020.115540>
- [11] Chin, Wen Jun, Kai Sheng See, Yu Han Ng, Jie Ling Gan, and Sing Yee Lim. "Technologies for Indoor Noise Attenuation: A Short Review." *Progress in Energy and Environment* (2019): 1-10.
- [12] Gély, Denis, and Gareth J. Bennett. "Aeroacoustics research in Europe: The CEAS-ASC report on 2018 highlights." *Journal of Sound and Vibration* 463 (2019): 114950. <https://doi.org/10.1016/j.jsv.2019.114950>
- [13] World Health Organization. *Environmental noise guidelines for the European region*. World Health Organization. Regional Office for Europe, 2018.
- [14] Uppu, Shiva Prasad, and Naren Shankar Radha Krishnan. "Turbulent Airflows over Serrated Wings: A Review on Experimental and Numerical Analysis." *Journal of Advanced Research in Fluid Mechanics and Thermal Sciences* 109, no. 1 (2023): 27-40. <https://doi.org/10.37934/arfmts.109.1.2740>
- [15] Ibren, Mohamed, Amelda Dianne Andan, Waqar Asrar, and Erwin Sulaeman. "A Review on Generation and Mitigation of Airfoil Self-Induced Noise." *Journal of Advanced Research in Fluid Mechanics and Thermal Sciences* 90, no. 1 (2022): 163-178. <https://doi.org/10.37934/arfmts.90.1.163178>
- [16] Kroeger, Richard A., H. D. Gruschka, and Tibor C. Helvey. *Low speed aerodynamics for ultra-quiet flight*. Air Force Flight Dynamics Laboratory, Air Force Systems Command, United States Air Force, 1972. <https://doi.org/10.1063/5.0012958>
- [17] Sarradj, Ennes, Christoph Fritzsche, and Thomas Geyer. "Silent owl flight: bird flyover noise measurements." *AIAA journal* 49, no. 4 (2011): 769-779. <https://doi.org/10.2514/1.J050703>
- [18] Graham, R. R. "The silent flight of owls." *The Aeronautical Journal* 38, no. 286 (1934): 837-843. <https://doi.org/10.1017/S0368393100109915>
- [19] Herr, Michaela, Karl-Stephane Rossignol, Jan Delfs, Nicolas Lippitz, and Michael Mößner. "Specification of porous materials for low-noise trailing-edge applications." In *20th AIAA/CEAS aeroacoustics conference*, p. 3041. 2014. <https://doi.org/10.2514/6.2014-3041>
- [20] Sandberg, R. D., L. E. Jones, N. D. Sandham, and P. F. Joseph. "Direct numerical simulations of tonal noise generated by laminar flow past airfoils." *Journal of Sound and Vibration* 320, no. 4-5 (2009): 838-858. <https://doi.org/10.1016/j.jsv.2008.09.003>
- [21] Andan, Amelda Dianne, and Duck-Joo Lee. "Discrete Tonal Noise of NACA0015 Airfoil at Low Reynolds Number." *Journal of Advanced Research in Fluid Mechanics and Thermal Sciences* 53, no. 1 (2019): 129-145.
- [22] Rossian, Lennart, Roland Ewert, and Jan W. Delfs. "Numerical investigation of porous materials for trailing edge noise reduction." *International Journal of Aeroacoustics* 19, no. 6-8 (2020): 347-364. <https://doi.org/10.1177/1475472X20954410>
- [23] Lee, Seongkyu, and Jessica G. Shum. "Prediction of airfoil trailing-edge noise using empirical wall-pressure spectrum models." *AIAA Journal* 57, no. 3 (2019): 888-897. <https://doi.org/10.2514/1.J057787>
- [24] Oberai, Assad A., Farzam Roknaldin, and Thomas JR Hughes. "Computation of trailing-edge noise due to turbulent flow over an airfoil." *AIAA journal* 40, no. 11 (2002): 2206-2216. <https://doi.org/10.2514/2.1582>
- [25] Wang, Meng, and Parviz Moin. "Computation of trailing-edge flow and noise using large-eddy simulation." *AIAA journal* 38, no. 12 (2000): 2201-2209. <https://doi.org/10.2514/2.895>
- [26] Wagner, Siegfried, Rainer Bareiss, and Gianfranco Guidati. *Wind turbine noise*. Springer Science & Business Media, 2012.
- [27] Afshari, Abbas, Ali A. Dehghan, and Mahdi Azarpeyvand. "Novel three-dimensional surface treatments for trailing-edge noise reduction." *AIAA Journal* 57, no. 10 (2019): 4527-4535. <https://doi.org/10.2514/1.J058586>
- [28] Moreau, Danielle J., Laura A. Brooks, and Con J. Doolan. "The effect of boundary layer type on trailing edge noise from sharp-edged flat plates at low-to-moderate Reynolds number." *Journal of Sound and Vibration* 331, no. 17 (2012): 3976-3988. <https://doi.org/10.1016/j.jsv.2012.04.016>

- [29] Chen, Nanshu, Hanru Liu, Qian Liu, Xingyu Zhao, and Yangang Wang. "Effects and mechanisms of LES and DDES method on airfoil self-noise prediction at low to moderate Reynolds numbers." *AIP Advances* 11, no. 2 (2021). <https://doi.org/10.1063/5.0038183>
- [30] Lee, Seongkyu. "The effect of airfoil shape on trailing edge noise." *Journal of Theoretical and Computational Acoustics* 27, no. 02 (2019): 1850020. <https://doi.org/10.1142/S2591728518500202>
- [31] Oerlemans, Stefan, Pieter Sijtsma, and B. Méndez López. "Location and quantification of noise sources on a wind turbine." *Journal of sound and vibration* 299, no. 4-5 (2007): 869-883. <https://doi.org/10.1016/j.jsv.2006.07.032>
- [32] Brooks, Thomas F., D. Stuart Pope, and Michael A. Marcolini. *Airfoil self-noise and prediction*. No. L-16528. 1989.
- [33] Moreau, Danielle J., and Con J. Doolan. "Noise-reduction mechanism of a flat-plate serrated trailing edge." *AIAA journal* 51, no. 10 (2013): 2513-2522. <https://doi.org/10.2514/1.J052436>
- [34] Barone, Matthew Franklin. "Survey of techniques for reduction of wind turbine blade trailing edge noise." (2011). <https://doi.org/10.2172/1029824>
- [35] Hubbard, Harvey H. "Aeroacoustics of flight vehicles: Theory and practice. volume 1. noise sources." *NASA reference publication* 1258 (1991).
- [36] Gregory, Nigel, and C. L. O'reilly. "Low-speed aerodynamic characteristics of NACA 0012 aerofoil section, including the effects of upper-surface roughness simulating hoar frost." (1970).
- [37] Oerlemans, Stefan, and Gerard Schepers. "Prediction of wind turbine noise directivity and swish." In *Third International Meeting on Wind Turbine Noise*, pp. 17-19. 2009.
- [38] Amiet, Roy K. "Noise due to turbulent flow past a trailing edge." *Journal of sound and vibration* 47, no. 3 (1976): 387-393. [https://doi.org/10.1016/0022-460X\(76\)90948-2](https://doi.org/10.1016/0022-460X(76)90948-2)
- [39] Howe, Michael S. "Trailing edge noise at low Mach numbers." *Journal of Sound and Vibration* 225, no. 2 (1999): 211-238. <https://doi.org/10.1006/jsvi.1999.2236>
- [40] Gruber, Mathieu, Phillip Joseph, and Mahdi Azarpeyvand. "An experimental investigation of novel trailing edge geometries on airfoil trailing edge noise reduction." In *19th AIAA/CEAS aeroacoustics conference*, p. 2011. 2013. <https://doi.org/10.2514/6.2013-2011>
- [41] Lyu, Benshuai, Mahdi Azarpeyvand, and Samuel Sinayoko. "Prediction of noise from serrated trailing edges." *Journal of Fluid Mechanics* 793 (2016): 556-588. <https://doi.org/10.1017/jfm.2016.132>
- [42] Stalnov, Oksana, Paruchuri Chaitanya, and Phillip F. Joseph. "Towards a non-empirical trailing edge noise prediction model." *Journal of Sound and Vibration* 372 (2016): 50-68. <https://doi.org/10.1016/j.jsv.2015.10.011>
- [43] Chase, David M. "Noise radiated from an edge in turbulent flow." *AIAA journal* 13, no. 8 (1975): 1041-1047. <https://doi.org/10.2514/3.60502>
- [44] Williams, JE Ffowcs, and L. H. Hall. "Aerodynamic sound generation by turbulent flow in the vicinity of a scattering half plane." *Journal of fluid mechanics* 40, no. 4 (1970): 657-670. <https://doi.org/10.1017/S0022112070000368>
- [45] Howe, Michael S. "A review of the theory of trailing edge noise." *Journal of sound and vibration* 61, no. 3 (1978): 437-465. [https://doi.org/10.1016/0022-460X\(78\)90391-7](https://doi.org/10.1016/0022-460X(78)90391-7)
- [46] Brooks, Thomas F., and T. H. Hodgson. "Trailing edge noise prediction from measured surface pressures." *Journal of sound and vibration* 78, no. 1 (1981): 69-117. [https://doi.org/10.1016/S0022-460X\(81\)80158-7](https://doi.org/10.1016/S0022-460X(81)80158-7)
- [47] Avallone, F., W. C. P. Van Der Velden, D. Ragni, and D. Casalino. "Noise reduction mechanisms of sawtooth and combed-sawtooth trailing-edge serrations." *Journal of Fluid Mechanics* 848 (2018): 560-591. <https://doi.org/10.1017/jfm.2018.377>
- [48] Jones, L. E., and R. D. Sandberg. "Acoustic and hydrodynamic analysis of the flow around an aerofoil with trailing-edge serrations." *Journal of Fluid Mechanics* 706 (2012): 295-322. <https://doi.org/10.1017/jfm.2012.254>
- [49] Arce León, Carlos, Roberto Merino-Martínez, Daniele Ragni, Francesco Avallone, and Mirjam Snellen. "Boundary layer characterization and acoustic measurements of flow-aligned trailing edge serrations." *Experiments in fluids* 57 (2016): 1-22. <https://doi.org/10.1007/s00348-016-2272-z>
- [50] Avallone, Francesco, Stefan Pröbsting, and Daniele Ragni. "Three-dimensional flow field over a trailing-edge serration and implications on broadband noise." *Physics of Fluids* 28, no. 11 (2016). <https://doi.org/10.1063/1.4966633>
- [51] Dassen, T., R. Parchen, J. Bruggeman, and F. Hagg. "Results of a wind tunnel study on the reduction of airfoil self-noise by the application of serrated blade trailing edges." (1996).
- [52] Oerlemans, Stefan, Murray Fisher, Thierry Maeder, and Klaus Kögler. "Reduction of wind turbine noise using optimized airfoils and trailing-edge serrations." *AIAA journal* 47, no. 6 (2009): 1470-1481. <https://doi.org/10.2514/1.38888>
- [53] Gruber, Mathieu. "Airfoil noise reduction by edge treatments." PhD diss., University of Southampton, 2012.
- [54] Chong, Tze Pei, and Alexandros Vathylakis. "On the aeroacoustic and flow structures developed on a flat plate with a serrated sawtooth trailing edge." *Journal of Sound and Vibration* 354 (2015): 65-90. <https://doi.org/10.1016/j.jsv.2015.05.019>

- [55] León, Carlos Arce, Roberto Merino-Martínez, Daniele Ragni, Francesco Avallone, Fulvio Scarano, Stefan Pröbsting, Mirjam Snellen, Dick G. Simons, and Jesper Madsen. "Effect of trailing edge serration-flow misalignment on airfoil noise emissions." *Journal of Sound and Vibration* 405 (2017): 19-33. <https://doi.org/10.1016/j.jsv.2017.05.035>
- [56] Avallone, Francesco, Stefan Pröbsting, and Daniele Ragni. "Three-dimensional flow field over a trailing-edge serration and implications on broadband noise." *Physics of Fluids* 28, no. 11 (2016). <https://doi.org/10.1063/1.4966633>
- [57] Gruber, Mathieu, Phillip Joseph, and Tze Chong. "On the mechanisms of serrated airfoil trailing edge noise reduction." In *17th AIAA/CEAS aeroacoustics conference (32nd AIAA aeroacoustics conference)*, p. 2781. 2011. <https://doi.org/10.2514/6.2011-2781>
- [58] Jaworski, Justin W., and Nigel Peake. "Aeroacoustics of silent owl flight." *Annual Review of Fluid Mechanics* 52 (2020): 395-420. <https://doi.org/10.1146/annurev-fluid-010518-040436>
- [59] Szóke, Máté, Daniele Fiscaletti, and Mahdi Azarpeyvand. "Uniform flow injection into a turbulent boundary layer for trailing edge noise reduction." *Physics of Fluids* 32, no. 8 (2020). <https://doi.org/10.1063/5.0013461>
- [60] Geyer, Thomas, Ennes Sarradj, and Christoph Fritzsche. "Measurement of the noise generation at the trailing edge of porous airfoils." *Experiments in fluids* 48 (2010): 291-308. <https://doi.org/10.1007/s00348-009-0739-x>
- [61] Bae, Youngmin, and Young J. Moon. "Effect of passive porous surface on the trailing-edge noise." *Physics of Fluids* 23, no. 12 (2011). <https://doi.org/10.1063/1.3662447>
- [62] Ali, Syamir Alihan Showkat, Mahdi Azarpeyvand, and Carlos Roberto Ilário Da Silva. "Trailing-edge flow and noise control using porous treatments." *Journal of Fluid Mechanics* 850 (2018): 83-119. <https://doi.org/10.1017/jfm.2018.430>
- [63] Finez, Arthur, Marc Jacob, Emmanuel Jondeau, and Michel Roger. "Broadband noise reduction with trailing edge brushes." In *16th AIAA/CEAS aeroacoustics conference*, p. 3980. 2010. <https://doi.org/10.2514/6.2010-3980>
- [64] Herr, Michaela, and Werner Dobrzynski. "Experimental Investigations in Low-Noise Trailing Edge Design." *AIAA journal* 43, no. 6 (2005): 1167-1175. <https://doi.org/10.2514/1.11101>
- [65] Clark, Ian A., W. Nathan Alexander, William Devenport, Stewart Glegg, Justin W. Jaworski, Conor Daly, and Nigel Peake. "Bioinspired trailing-edge noise control." *AIAA Journal* 55, no. 3 (2017): 740-754. <https://doi.org/10.2514/1.J055243>
- [66] Jawahar, Hasan Kamliya, Qing Ai, and Mahdi Azarpeyvand. "Experimental and numerical investigation of aerodynamic performance for airfoils with morphed trailing edges." *Renewable Energy* 127 (2018): 355-367. <https://doi.org/10.1016/j.renene.2018.04.066>
- [67] Talboys, Edward, Thomas F. Geyer, and Christoph Brücker. "An aeroacoustic investigation into the effect of self-oscillating trailing edge flaplets." *Journal of Fluids and Structures* 91 (2019): 102598. <https://doi.org/10.1016/j.jfluidstructs.2019.02.014>
- [68] Chong, Tze Pei, and Phillip F. Joseph. "An experimental study of airfoil instability tonal noise with trailing edge serrations." *Journal of Sound and Vibration* 332, no. 24 (2013): 6335-6358. <https://doi.org/10.1016/j.jsv.2013.06.033>
- [69] León, Carlos Arce, Roberto Merino-Martínez, Daniele Ragni, Francesco Avallone, Fulvio Scarano, Stefan Pröbsting, Mirjam Snellen, Dick G. Simons, and Jesper Madsen. "Effect of trailing edge serration-flow misalignment on airfoil noise emissions." *Journal of Sound and Vibration* 405 (2017): 19-33. <https://doi.org/10.1016/j.jsv.2017.05.035>
- [70] Chong, T. P., P. F. Joseph, and M. Gruber. "Airfoil self noise reduction by non-flat plate type trailing edge serrations." *Applied Acoustics* 74, no. 4 (2013): 607-613. <https://doi.org/10.1016/j.apacoust.2012.11.003>
- [71] Bohn, A. J. "Edge noise attenuation by porous-edge extensions." In *14th aerospace sciences meeting*, p. 80. 1976. <https://doi.org/10.2514/6.1976-80>
- [72] Potter, C. *An experiment to examine the effect of porous trailing edges on the sound generated by blades in an airflow*. American Institute of Aeronautics and Astronautics, 1968.
- [73] Herr, Michaela, and Johann Reichenberger. "In search of airworthy trailing-edge noise reduction means." In *17th AIAA/CEAS Aeroacoustics Conference (32nd AIAA Aeroacoustics Conference)*, p. 2780. 2011. <https://doi.org/10.2514/6.2011-2780>
- [74] Sarradj, Ennes, and Thomas Geyer. "Noise generation by porous airfoils." In *13th AIAA/CEAS Aeroacoustics Conference (28th AIAA Aeroacoustics Conference)*, p. 3719. 2007. <https://doi.org/10.2514/6.2007-3719>
- [75] Geyer, Thomas, Ennes Sarradj, and Christoph Fritzsche. "Porous airfoils: noise reduction and boundary layer effects." *International journal of aeroacoustics* 9, no. 6 (2010): 787-820. <https://doi.org/10.1260/1475-472X.9.6.787>
- [76] Geyer, Thomas F., and Ennes Sarradj. "Trailing edge noise of partially porous airfoils." In *20th AIAA/CEAS aeroacoustics conference*, p. 3039. 2014. <https://doi.org/10.2514/6.2014-3039>
- [77] Zhang, Minghui, and Tze Pei Chong. "Experimental investigation of the impact of porous parameters on trailing-edge noise." *Journal of Sound and Vibration* 489 (2020): 115694. <https://doi.org/10.1016/j.jsv.2020.115694>

- [78] Geyer, Thomas Fritz, and Ennes Sarradj. "Self noise reduction and aerodynamics of airfoils with porous trailing edges." In *Acoustics*, vol. 1, no. 2, pp. 393-409. MDPI, 2019. <https://doi.org/10.3390/acoustics1020022>
- [79] Revell, James, James Revell, Herbert Kuntz, Frank Balena, Clifton Horne, Bruce Storms, Robert Dougherty *et al.*, "Trailing-edge flap noise reduction by porous acoustic treatment." In *3rd AIAA/CEAS aeroacoustics conference*, p. 1646. 1997. <https://doi.org/10.2514/6.1997-1646>
- [80] Bernicke, Paul, R. A. D. Akkermans, Varun B. Ananthan, Roland Ewert, Jürgen Dierke, and Lennart Rossian. "A zonal noise prediction method for trailing-edge noise with a porous model." *International Journal of Heat and Fluid Flow* 80 (2019): 108469. <https://doi.org/10.1016/j.ijheatfluidflow.2019.108469>
- [81] Wagner, Claus, Thomas Hüttl, and Pierre Sagaut, eds. *Large-eddy simulation for acoustics*. Vol. 20. Cambridge University Press, 2007. <https://doi.org/10.1017/CBO9780511546143>
- [82] Storey, R. C., S. E. Norris, and J. E. Cater. "Modelling turbine loads during an extreme coherent gust using large eddy simulation." In *Journal of Physics: Conference Series*, vol. 524, no. 1, p. 012177. IOP Publishing, 2014. <https://doi.org/10.1088/1742-6596/524/1/012177>
- [83] Kim, Sung-Eun. "Large eddy simulation using an unstructured mesh based finite-volume solver." In *34th AIAA fluid dynamics conference and exhibit*, p. 2548. 2004. <https://doi.org/10.2514/6.2004-2548>
- [84] Smagorinsky, Joseph. "General circulation experiments with the primitive equations: I. The basic experiment." *Monthly weather review* 91, no. 3 (1963): 99-164. [https://doi.org/10.1175/1520-0493\(1963\)091<0099:GCEWTP>2.3.CO;2](https://doi.org/10.1175/1520-0493(1963)091<0099:GCEWTP>2.3.CO;2)
- [85] Germano, Massimo, Ugo Piomelli, Parviz Moin, and William H. Cabot. "A dynamic subgrid-scale eddy viscosity model." *Physics of Fluids A: Fluid Dynamics* 3, no. 7 (1991): 1760-1765. <https://doi.org/10.1063/1.857955>
- [86] Zhao, Dan, Nuomin Han, Ernest Goh, John Cater, and Arne Reinecke. *Wind turbines and aerodynamics energy harvesters*. Academic Press, 2019.
- [87] Lighthill, Michael James. "On sound generated aerodynamically I. General theory." *Proceedings of the Royal Society of London. Series A. Mathematical and Physical Sciences* 211, no. 1107 (1952): 564-587. <https://doi.org/10.1098/rspa.1952.0060>
- [88] Lighthill, Michael James. "On sound generated aerodynamically II. Turbulence as a source of sound." *Proceedings of the Royal Society of London. Series A. Mathematical and Physical Sciences* 222, no. 1148 (1954): 1-32. <https://doi.org/10.1098/rspa.1954.0049>
- [89] Williams, JE Ffowcs, and David L. Hawkings. "Sound generation by turbulence and surfaces in arbitrary motion." *Philosophical Transactions for the Royal Society of London. Series A, Mathematical and Physical Sciences* (1969): 321-342. <https://doi.org/10.1098/rsta.1969.0031>
- [90] Shen, Wen Zhong, Weijun Zhu, and Jens Nørkær Sørensen. "Aeroacoustic computations for turbulent airfoil flows." *AIAA journal* 47, no. 6 (2009): 1518-1527. <https://doi.org/10.2514/1.40399>